The effect of sintering temperature on the properties of the BiOCl films for potential application in DSSC

L. Pizarro-Castillo[1], Adriana C. Mera[2,3], G. Cabello-Guzmán[4], C. Bernal[2,5], M. Bizarro[6], C. Carrasco[1], María-Jesús Blesa[7], C. A. Rodríguez[2,3*]

1 Thin film and electrochemical processes laboratory, Department of Materials Engineering, Faculty of Engineering, Universidad de Concepción. 270 Edmundo Larenas St., Concepción 4070409, Chile.

2 Multidisciplinary Research Institute for Science and Technology, Universidad de La Serena, 1305 Raúl Bitrán Av., La Serena, 1700000, Chile.

3 Department of Chemistry, Faculty of Science, Universidad de La Serena, 1305 Raúl Bitrán Av., La Serena, 1700000, Chile.

4 *Department of Basic Sciences, Faculty of Sciences, Universidad del Bío-Bío, Campus Fernando May, 720 Andres Bello St., 3784444, Chillán, Chile.*

5 Departamento de Ingeniería de Alimentos, Facultad de Ingeniería, Universidad de La Serena, 1305 Raúl Bitrán Av., La Serena, 1700000, Chile.

6 Instituto de Investigaciones en Materiales, Universidad Nacional Autónoma de México, Circuito Exterior S/N, Ciudad Universitaria, Coyoacán, 04510, Ciudad de México, México.

7 Departamento de Química Orgánica, INMA, Universidad de Zaragoza-CSIC, 50009, Zaragoza, Spain.

** Corresponding author. E-mail address: arodriguez@userena.cl*

TEL:+56-9-84775538

Abstract

In this work, BiOCl films were obtained by tape casting using BiOCl powders synthesized by the co-precipitation method. The effect of the film's sintering temperature (300°C to 600°C) on the morphology, chemical composition, crystalline phases and optical characteristics was studied. The obtained BiOCl powders showed a flake-like morphology, a tetragonal crystalline structure without secondary phases and a wide band gap of 3.53 eV. For BiOCl films, results indicated that as the sintering temperature increased the flake-like shaped particles changed to rectangular ones while the amount of chlorine in the films decreased. A phase transition from tetragonal BiOCl to monoclinic $Bi_{24}O_{31}Cl_{10}$ was also observed as the sintering temperature increased. Consequently, optical studies revealed that the band gap of BiOCl films decreased from 3.03 eV to 2.82 eV. FTIR analysis demonstrated that the organic groups were removed from the films only for sintering temperatures above 400 °C. The Rhodamine B dye adsorption capacity of BiOCl films decreased with increasing sintering temperature. The results obtained allow us to conclude that BiOCl films are suitable for use in DSSC when the sintering temperature is in the range of 400 to 500 ºC.

Keywords: BiOCl films, tape casting, Dye-sensitized solar cells.

1. Introduction

Dye-sensitized solar cells (DSSC) have emerged as a simple and low-cost alternative to traditional silicon-based solar cells. So far, the highest Power Conversion Efficiency (PCE) for commonly TiO_2-based DSSC is close to 14.3 % [1]. **Increasing this value is one of the main challenges of DSSC devices for future industrial production. Hence,** new semiconductor materials capable of increasing the adsorption of dye molecules, reducing recombination processes and improving charge-carrier transport are needed [2]. Several semiconductors have been studied as a potential replacement for TiO_2, such as ZnO [3], SnO_2 [4], Nb_2O_5 [5] and $SrTiO_3$ [6]; **however, none of them has significantly improved the efficiency of TiO_2-based DSSC.**

Bismuth oxychloride (BiOCl) is a relatively new semiconductor material that has received much attention due to its similarity to TiO_2 [7]. BiOCl is an indirect semiconductor with a wide band gap (3.2 - 3.5 eV [8]) and a light absorption edge close to 360 nm that would ensure light transmission to the dye molecules if used in DSSC [9, 10]. **The internal structure of BiOCl consists of $[Bi_2O_2]^{2+}$ layers intercalated by two slabs of Cl atoms, which provides this material a favorable transfer and separation of photogenerated charge carriers [11]. This unique layered structure gives the material excellent physical and chemical properties, allowing its application in different fields such as solar cells, photocatalysts and photoelectrochemical studies [12, 13]. Furthermore, theoretical studies have shown that BiOCl exhibits suitable band edge positions to collect electrons from different organic compounds [14].**

Not only the optical and structural properties of the semiconductor are important for obtaining an efficient DSSC, but also the morphological characteristics play an important

role to evaluate the dye molecules adsorption [15]. It is known that semiconductor films used in DSSC must have a porous morphology for large adsorption of dye molecules on their surface **[16].** Although several physical and chemical methods are available to obtain semiconductor films, most of them lead to compact morphology instead of a porous one **[17].** Commonly, the synthesis of porous semiconductor films for DSSC application is carried out employing the Screen Printing method [18, 19] or Tape Casting [20]. In these two methods, an annealing process is required **to tune the particle size and phase composition, which ultimately determines the textural material properties. Therefore, the study of the effect of the annealing process on the film properties is crucial to controlling both the composition and the morphology of the film for DSSC application.**

As far as we know, only few works have reported the synthesis and use of BiOCl films as a semiconductor material in DSSCs [21, 22]. Some attempts have been done for this purpose. **Luz et al. obtained BiOCl and BiOBr nanodiscs (100-150 nm in diameter, 15-25 nm in thickness) by water-based nucleation. In order to control particle growth and shape particles, the nanodiscs were purified by a complex phase-transfer reaction. The prepared BiOCl film was used in a p-DSSC device sensitized with coumarin and a PCE of 0.003% was achieved** [21]. In 2014, Wang et al. reported a DSSC based on the $Bi_{24}O_{31}Cl_{10}$ semiconductor sensitized with the N719 dye. **Nevertheless, this material exhibited a relatively low band gap of 2.2 eV, which lead to an absorption of visible light, limiting the light absorption by dye molecules [22]. Hence, the challenge of obtaining BiOCl films with suitable characteristics to be used in DSSCs remains.**

The aim of this paper is to study the effect of sintering temperature on the BiOCl properties to be used as a semiconductor in DSSC. BiOCl powder was synthesized by a

simple co-precipitation method and films were obtained by the tape-casting method. These films were heat-treated at temperatures of 300°C, 400°C, 500°C and 600 °C. Morphology, microstructure and optical characteristics of BiOCl films are measured and related to the adsorption of dye molecules, specifically, Rhodamine B.

2. Experimental Details

2.1 Synthesis of BiOCl powder

BiOCl powder was synthetized by the co-precipitation method according to the procedure represented in Figure 1 a) to c). **0.29 g of KCl (99.0 %, Merck®) was dissolved in 40 mL of deionized water and stirred for 30 min. A second solution containing 1.97 g of $Bi(NO_3)_3\times 5H_2O$ (99.0 %, Sigma-Aldrich®) was dissolved in 40 mL of 10 % acetic acid solution and stirred for 30 min (see Fig. 1 a). Subsequently, the KCl solution (4 mM) was added dropwise to the bismuth solution (4 mM) under stirring (Fig. 1 b).** After the total incorporation of both solutions, the reaction mixture was kept under constant stirring for 30 min at room temperature. The resulting product was collected by gravity filtration and washed **with** ethanol and deionized water **successively**. The resulting powder was dried at 60 °C for 12 h (Fig. 1c) [23].

2.2 Synthesis of BiOCl films

BiOCl films were deposited on glass substrates using the tape-casting technique. **First, the** substrates were cleaned with water and soap and subsequently rinsed with deionized water and ethanol. Cleaned substrates were dried in an oven at 60 °C for 30 min. **Then, to deposit the BiOCl film, an exposed area of 0.5 × 0.5 cm was delimited by using Kapton tape®.**

Secondly, the BiOCl paste was prepared by mixing 0.5 g of BiOCl powder, 0.4 g of polyvinylpyrrolidone (PVP, 10.000 mol wt, Sigma-Aldrich®) and 0.7 mL of ethanol (99.5%, Emplura®) as graphically shown in Fig. 1 d). After 15 min of continuous mixing, 0.3 mL of α-terpineol (96%, Sigma-Aldrich®) was added and mixed for 5 min (Fig. 1 e). Afterward, as shown in Fig. 1 f), the paste was deposited on the glass substrate by spreading it on the substrate surface with a squeegee.

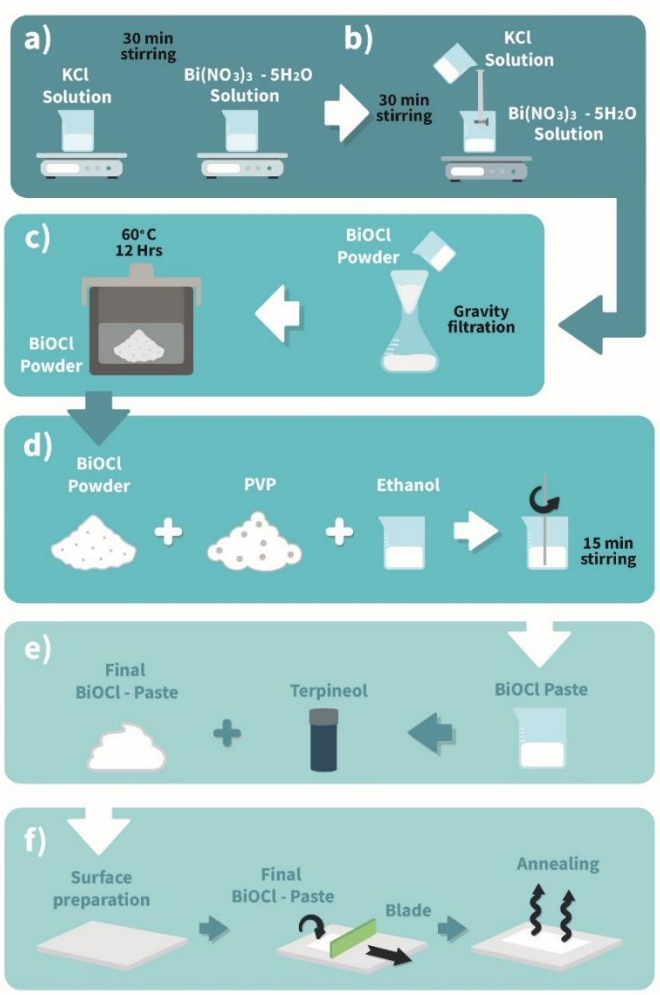

Fig. 1. Synthesis of a) to c) BiOCl powder by co-precipitation method; d) to f) BiOCl films by tape casting.

The obtained samples were kept at room temperature for 5 min, and after, the Kapton tape was removed. The obtained samples were sintered in air in a tubular furnace (MPTI corporation GSL–1100X).

Four different sintering conditions were tested, which are shown in Table 1. **These temperatures of sintering were selected to eliminate organic additives and solvents used during the BiOCl films synthesis [19].** The sintered samples were removed from the furnace when the temperature was lower than 50 °C and stored in dry and dark conditions.

Table 1. Sintering conditions for BiOCl films

Experiment Nº	**Sample**	**Temperature (ºC)**	**Time (min)**
1	BiOCl 300	300	180
2	BiOCl 400	400	180
3	BiOCl 500	500	30
4	BiOCl 600	600	30

2.3 Characterization of BiOCl powders and films

Surface characteristics and semi-quantitative chemical composition of the BiOCl samples were evaluated using scanning electron microscopy (SEM) and energy dispersive spectroscopy (EDS), using a Hitachi Su 70 microscope with an EDS detector attached to the equipment. The specific surface area and the pore size distribution of the samples were obtained by N_2 adsorption–desorption analysis, using a Micromeritics ASAP 2020 instrument and applying Brunauer-Enmmets-Teller (BET) and Barret-

Joyner-Halenda (BJH) methods. The crystalline phases of BiOCl powders and films were identified by X-ray diffraction (XRD) using a Rigaku Ultim IV diffractometer with Cu Kα radiation (λ = 1.5406 A). The samples were measured at the scanning rate of 0.5°/min in the 2θ scan range of 5° - 65° at 40 kV and 40 mA. Optical characteristics of the obtained samples were studied through diffuse reflectance spectroscopy (DRS) in the wavelength interval of 340–800 nm using a UV-Vis spectrophotometer Thermo Scientific model Evolution 220; the optical band gap was calculated through the Kubelka-Munk method [24]. Finally, Fourier transform infrared (FTIR) spectra were obtained using a PerkinElmer spectrometer model Spectrum Two with $LiTaO_3$ MIR detector.

2.4 Dye adsorption studies on BiOCl films

The dye adsorption capability of the BiOCl films was investigated with the method previously reported by Marco *et al*. by the absorbance spectra of sensitized transparent BiOCl films [25]. Glass substrates with an exposed area of 2.5 × 2.5 cm^2 were cleaned as described in section 2.2. Subsequently, 250 μL of BiOCl paste (0.5 g of BiOCl powder, 0.4 g of PVP, 1.5 mL of ethanol and 0.3 mL of α-terpineol) was spread on the glass substrate by tape casting. The obtained transparent films were sintered at the conditions detailed in Table 1.

For dye adsorption, the obtained transparent BiOCl films were immersed in a Rhodamine B solution (1.37×10^{-3} M) for 8, 12 and 24 h. After the corresponding time, samples were removed from the solution, washed with ethanol, and dried at room temperature. Dye-sensitized BiOCl samples were kept in dark conditions to avoid dye degradation. Absorption

spectra of sensitized BiOCl films were measured in the wavelength interval of 340–800 nm using a UV-VIS spectrophotometer ThermoScientific Evolution 220.

3. Results and Discussion

3.1. Characterization of BiOCl powder

Figure 2 a) shows the SEM images for the BiOCl powder obtained by the co-precipitation method, where flake-like shape particles are observed. It can also be seen that the flakes are forming agglomerates with a size of ~ 1μm. Deng *et al*. and Ma *et al*. reported similar morphology for BiOCl powder obtained by the co-precipitation method [26, 27]. The semi-quantitative chemical composition of the BiOCl powder, measured by EDS, showed the presence of Bi (38.1%), O (24.1%) and Cl (37.8%) with a Bi:O:Cl ratio of 1:0.7:1 that could mean that samples have oxygen vacancies.

Figure 2 b) shows the XRD diffractograms, where the polycrystalline nature of the obtained BiOCl powder can be seen. Peak identification reveals the tetragonal phase of BiOCl according to the Powder Diffraction File (PDF) from the International Centre for Diffraction Data (ICDD) N° 06-0249 [28,29]. A peak widening is observed, which can be attributed to small crystallite size and/or inhomogeneous deformations in the powders. To determine the reason for the widening of the peaks, Williamson-Hall (W-H) relation was applied, which is given by Eq. (1) [30]:

$$\beta \cos\theta = \frac{K\lambda}{D} + 4\varepsilon sin\theta \qquad (1)$$

where D is the average crystallite size, λ is the X-ray wavelength (0.154056 nm), k is the shape factor (0.75 in this case [31]), β is the full width at half maximum (FWHM) of the diffraction peaks, ε is the lattice microstrain and θ is the diffraction angle.

Figure 2 c) shows the Williamson-Hall plot, which is obtained by plotting $4\sin(\theta)$ along the *x*-axis and $\beta\cos(\theta)$ along the *y*-axis. From the linear fit to the data, the crystallite size was estimated from the *y*-intercept and the lattice strain from the slope. The obtained value for D was 22 nm which indicates the nanocrystalline nature of the synthesized BiOCl powders. **The microstrain was found to be 1.75×10^{-3}, indicating that the lattice strain practically does not contribute to peak broadening** [28]. The presence of these lattice deformations could be a consequence of the oxygen atom vacancies revealed by EDS analysis.

The optical band gap of the BiOCl powder was calculated using the Tauc plot through the Kubeka-Munk model for diffuse reflectance [24]. Figure 2 d) shows the Tauc plot, where a band gap value of 3.53 ± 0.03 eV is extracted, which agrees with the value reported previously for BiOCl powders [29]. An optical band gap higher than 3.0 eV ensures that most of the incident light is not being absorbed by the semiconductor, which is an optimal condition to be considered as a potential photoanode in DSSC **[32].**

3.2. Characterization of BiOCl films

Figure 3 shows photographs of the BiOCl films before and after the heat treatments. **The obtained sample prior annealing process is shown in Fig. 3 a), where it is possible to observe a homogeneous and white film, which is characteristic of BiOCl material. In Fig. 3 b) it is shown that after sintering at 300 °C, a dark BiOCl film was obtained. This indicates that the organic additives and solvents used during the film deposition were not completely evaporated and/or burning during the heat treatment. The presence of these organic compounds reduces the exposition of the semiconductor surface to the dye molecules and blocks the light transmission towards the dye.** For this reason, this sample was discarded and not subjected to further characterization.

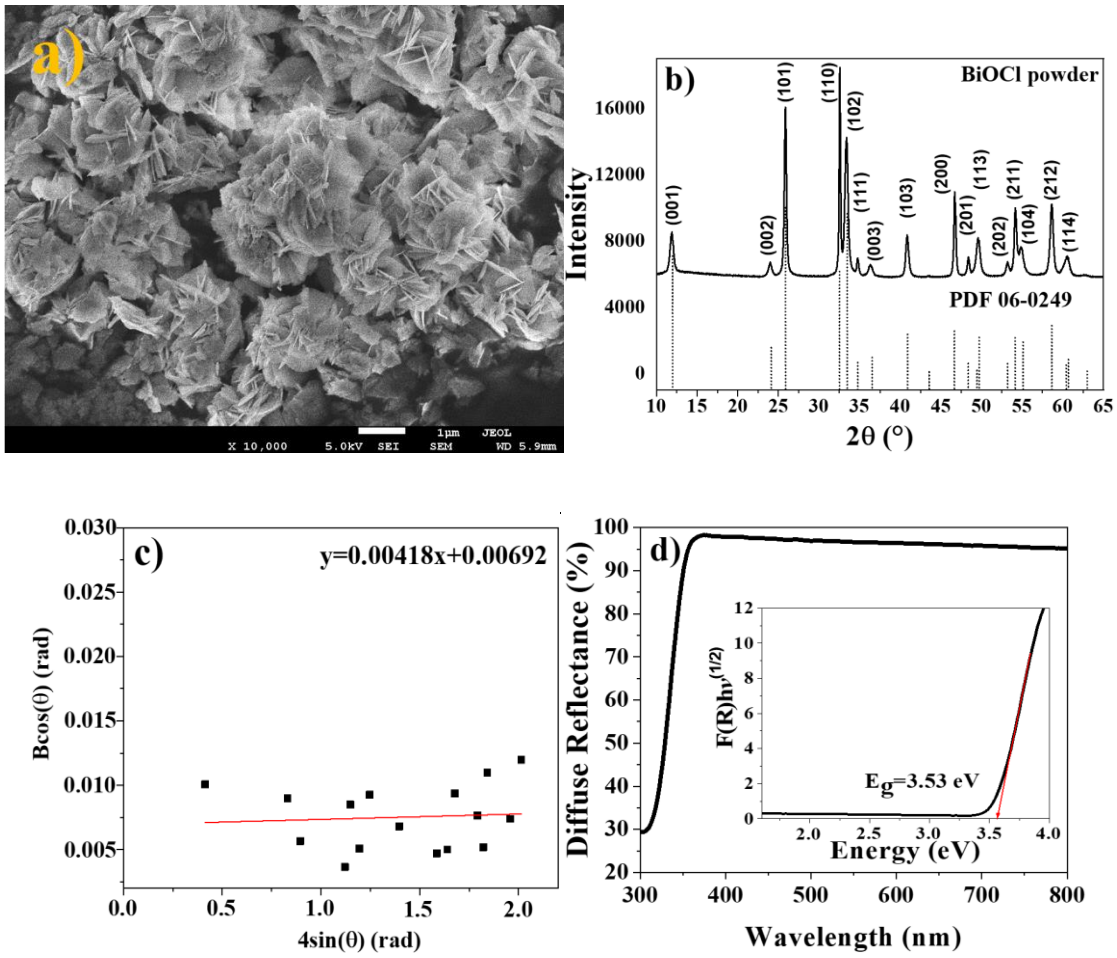

Fig. 2. BiOCl powder obtained by co-precipitation method: a) SEM image, b) XRD pattern, c) W-H plot, d) Tauc plot.

Fig. 3 c) depicts the BiOCl sample sintered at 400 °C where is seen that the obtained film exhibits a white color meaning that all the organic additives and solvents were removed after 3 h of calcination. **For samples sintered at 500 °C and 600 °C, Fig. 3 d and e, respectively, the films exhibited a white color after 30 min of annealing. From Fig. 3 c) to e), it can be seen the tendency** of the films to become slightly yellowish as the sintering temperature increases, which could be related to possible structural and/or chemical modifications.

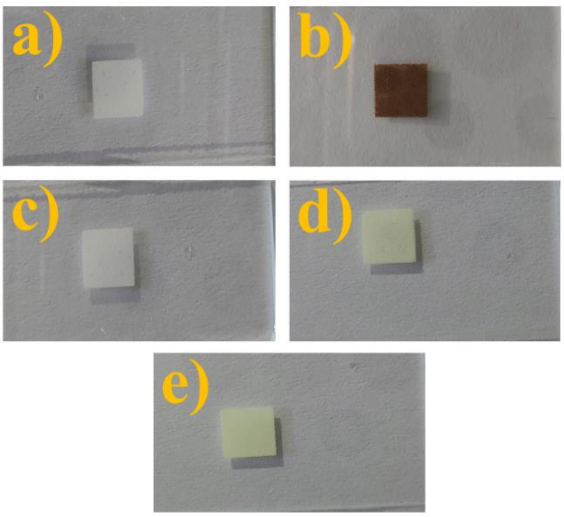

Fig. 3. BiOCl films: a) without heat treatment, heat treated at b) 300ºC (BiOCl 300), c) 400ºC (BiOCl 400), d) 500ºC (BiOCl 500) and d) 600ºC (BiOCl 600).

The surface morphology of the BiOCl films sintered at different temperatures is shown in Fig. 4. Figure 4 a) and b) show the surface characteristics of the BiOCl-400 sample. A highly porous morphology with flake-like shaped particles that are linked to each other forming spherical aggregates is observed. It can be noticed that the particle shape for the BiOCl-400 sample is similar to the one observed for the BiOCl powders. It is highlighted that the highly porous morphology observed would favor the dye molecules adsorption on the semiconductor surface.

The surface morphology of the BiOCl-500 sample is shown in Fig. 4 c) and d), where a more compact film than the BiOCl-400 sample is observed. In addition, some cracks are seen on the sample surface (see yellow arrow), which could be attributed to a possible phase transformation in the films involving crystalline structure changes and deformations [33, 34]. **Figure 4 e) and f) shows the morphology of the BiOCl-600 sample, where it is observed that the sintering at a temperature of 600 °C** leads to the appearance of broad cracks on

the sample surface. In addition, the flake-like shaped particles observed in the BiOCl-400 and BiOCl-500 samples changed to rectangular with rounded edges, resulting in a more compact surface. This morphological modification could be associated with the changes in the chemical composition of the films, which are shown in Table 2. The increase in temperature leads to a shrinkage of the films because of the reduction of chlorine in the samples, which corresponds with previous reports [20].

From Table 2, it is also observed that in all samples an increase in the sintering temperature produces a diminution in chlorine concentration.

To reach a further understanding of the effect of sintering temperature on the surface characteristics, the specific surface area of the BiOCl powders thermally treated at 400, 500 and 600º C was measured. It must be noted that the specific surface area on films is not possible to be measured, and the values for BiOCl powders are presented only for comparison purposes. The results showed that the specific surface area for BiOCl powder sintered at 400 °C, 500 °C and 600 °C were 17.05 ± 0.11, 19.55 ± 0.09 and 6.02 ± 0.07 m^2/g, respectively, and the pore volume was 0.054, 0.054 and 0.017 cm^3/g, respectively. Hence, the BiOCl annealed at 600 °C exhibited the lowest surface area, which is consistent with the morphological change observed in Fig. 4.

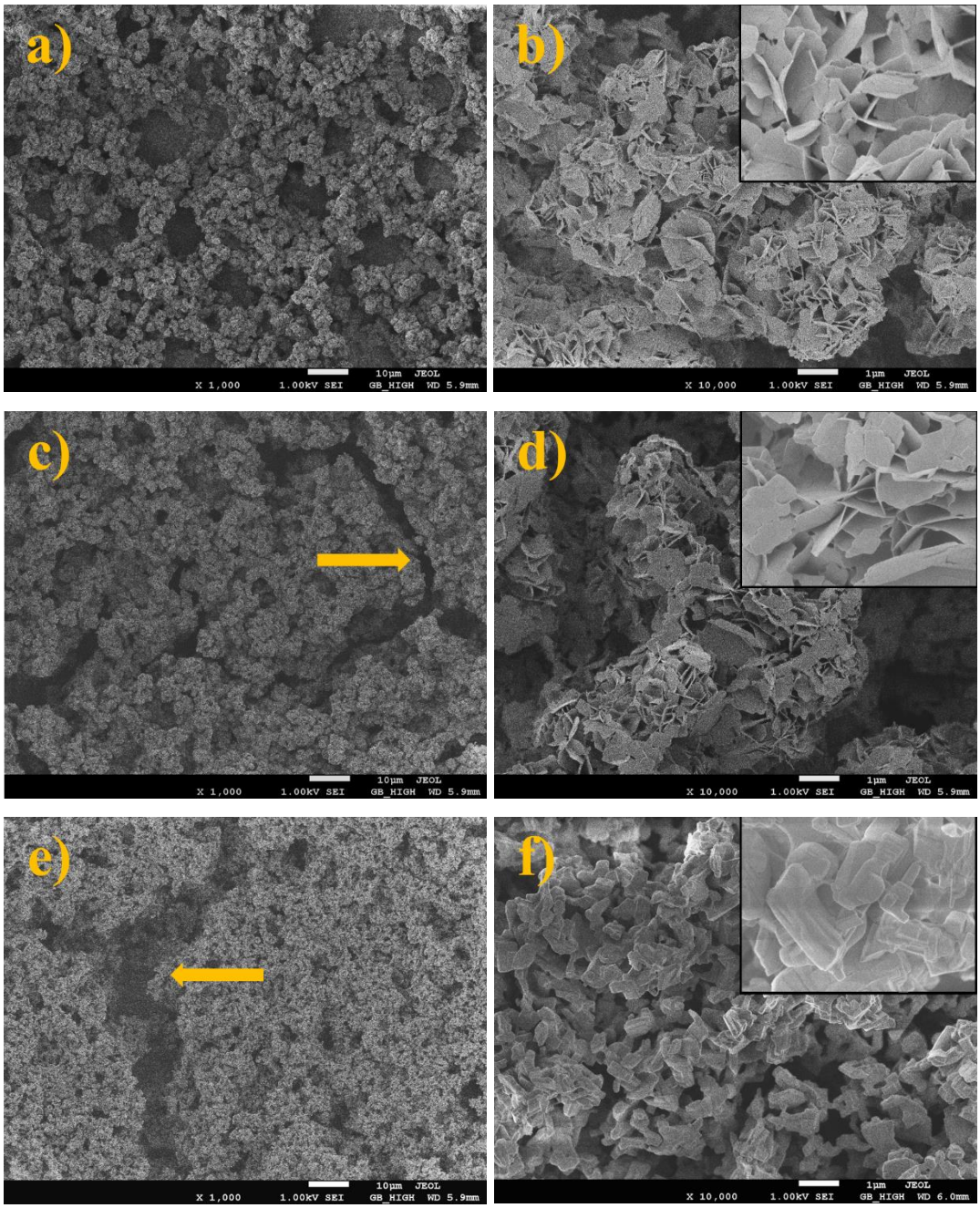

Fig. 4. SEM images of sintered BiOCl films at different temperatures: (a-b) 400 °C, (c-d) 500 °C and (e-f) 600 °C.

Table 2. Semi-quantitative EDS chemical composition of obtained sintered films.

Sample	**Bi (% at.)**	**O (% at.)**	**Cl (% at.)**	**Bi: O: Cl**
BiOCl 400 °C	35.7 ± 1.3	46.7 ± 1.9	17.6 ± 0.7	1: 1.30: 0.49
BiOCl 500 °C	38.7 ± 1.3	45.3 ± 1.9	16.0 ± 0.7	1: 1.17: 0.41
BiOCl 600 °C	40.3 ± 1.3	48.4 ± 1.9	11.3 ± 0.7	1: 1.20: 0.30

Figure 5 shows the XRD pattern of BiOCl films after sintering at (a) 400, (b) 500 and (c) 600 °C. From the diffractogram of the BiOCl-400 sample (Fig. 4 a), the presence of several diffraction peaks is observed, which can be ascribed to both the tetragonal phase of BiOCl (star symbol) according to the PDF N° 06-0249 and the tetragonal phase of Bi_2O_3 (circle symbol) according to the PDF N° 29-0236. The appearance of Bi_2O_3 is a consequence of the chlorine volatilization during the sintering process, and therefore the crystal phase becomes unstable undergoing a phase transformation from pure BiOCl to a mixture of Bi_2O_3 and BiOCl. [35].

When the sintering temperature is increased up to 500 °C (see Fig. 5 b), the appearance of several diffraction peaks is observed, which can be ascribed to the tetragonal phase of Bi_2O_3 according to the PDF N° 29-0236. When comparing the XRD pattern for BiOCl-400 with BiOCl-500 samples, a partial phase transformation from BiOCl to Bi_2O_3 is observed. This change could be attributed to the chlorine reduction during the sintering. It has been reported that, among their four polymorphs, the tetragonal phase of Bi_2O_3 is the predominant one after annealing at temperatures up to 643 °C [36], which agrees with the finding in these samples.

In Fig. 5 c) the XRD pattern for the BiOCl-600 sample is shown. It is possible to observe a drastic change in the diffraction pattern when the sintering temperature was 600 °C. The diffraction peaks can be attributed to the monoclinic phase of $Bi_{24}O_{31}Cl_{10}$ according to the PDF N° 75-0887. The phase transformation observed as the sintering temperature increases as a consequence of the continuous chlorine volatilization. Thus, the heat treatment allowed the continued reduction of chlorine to Cl_2, leading to a phase transformation in two stages: (a) the appearance of the Bi_2O_3 phase at 400°C and 500 °C, and (b) change from the tetragonal lattice of BiOCl to the monoclinic lattice of $Bi_{24}O_{31}Cl_{10}$ at 600 °C [11, 37]. These findings are in accordance with the atomic chemical composition shown in Table 2, where the atomic composition of the BiOCl-400 sample can be adjusted to a mixture of BiOCl (52.8 %) and Bi_2O_3 (47.2 %); similarly, the BiOCl-500 sample corresponds to a mixture of BiOCl (48 %) and Bi_2O_3 (52 %). On the contrary, the atomic composition of the BiOCl-600 sample corresponds only to the single phase of $Bi_{24}O_{31}Cl_{10}$.

The crystallite size of BiOCl films was calculated by using Scherrer's equation, due to films obtained at 400 ° and 500 °C were a mixture of Bi_2O_3 and BiOCl phases, thus the near position of peaks involve overlaps the points on the Williamson-Hall graph. The crystallite size values were 19, 13 and 30 nm for BiOCl samples annealed at 400 °C, 500 °C and 600 °C, respectively. This behavior could be attributed to the phase change from BiOCl to $Bi_{24}O_{31}Cl_{10}$ as the sintering temperature increased from 400 °C to 600 °C. The sample annealed at 500 °C exhibits a broadening peak with a reduction of the crystallite size as a consequence of the increase in lattice disorder, while at 600 °C an increase in the crystallite size was observed.

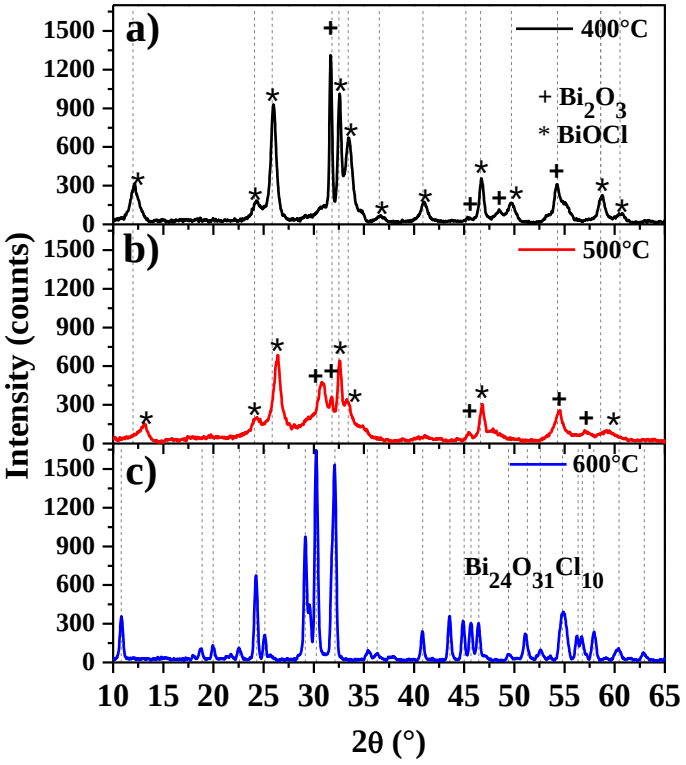

Fig 5. Diffraction patterns of films heat treated at (a) 400 °C, (b) 500 °C and (c) 600 °C.

Figure 6 shows the Tauc plot obtained from the diffuse reflectance spectra through the Kubelka-Munk method. By extrapolating the linear portion of the Tauc plot, the band gap values for BiOCl films are obtained, where it is seen that the band gap values tend to decrease as the sintering temperature increases. The reduction in the band gap can be attributed to the phase transformation with rising temperature. Thus, the BiOCl-400 sample has a band gap value of 3.03 ± 0.01 eV which agrees with the expected value for BiOCl [38, 39]. For the BiOCl-500 sample, the band gap value exhibits a reduction up to 2.87± 0.06 eV, which is very close to the band gap value for Bi_2O_3 (E_g=2.87) [40]. The BiOCl-600 sample exhibits a band gap value of 2.80± 0.01 eV, which agrees with the value for the $Bi_{24}O_{31}Cl_{10}$ phase (Eg=2.7-2.8 eV) [11, 36].

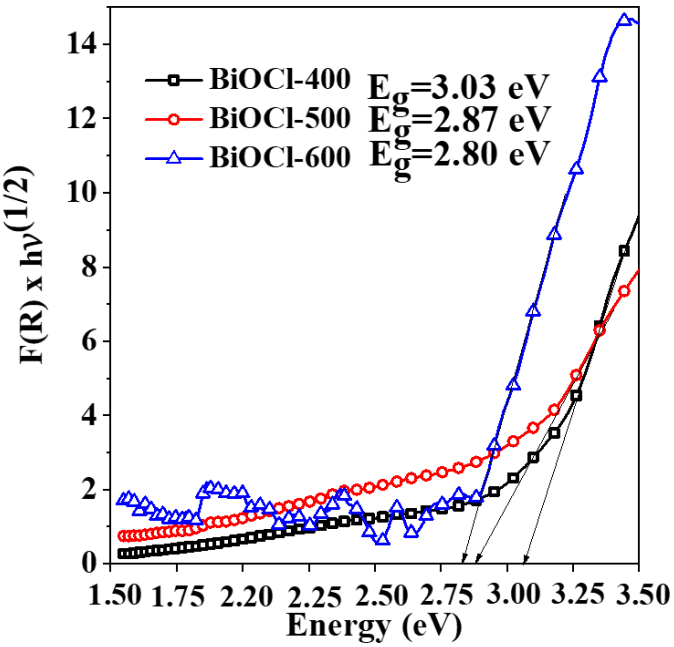

Fig. 6. Tauc plot of BiOCl films.

The FTIR spectra of BiOCl powder, BiOCl-400, BiOCl-500 and BiOCl-600 samples are presented in Fig. 7. All the samples showed the band at 530 cm^{-1}, which corresponds to the symmetrical stretching vibration of Bi-O bond [41-42]. The band at 650 cm^{-1} is also assigned to the Bi-O bond [41, 43], which increases with the annealing temperature and **is seen in** the sample annealed at 600 °C. The small band located at 1461 cm^{-1} in the powder sample is attributed to O-Cl vibration and the band slightly perceptible at 1165 cm^{-1} corresponds to the Bi-Cl bond. The signals at 530 and 650 cm^{-1} for the BiOCl-600 sample are observed to be more intense than BiOCl-400 and BiOCl-500 samples, which can be attributed to the phases present in the samples.

Moreover, it can be observed that the BiOCl powder sample contains some remaining organic groups from the precursors used during the co-precipitation method. **The bands at 1050 and 1320 cm^{-1} are ascribed to NO_3^- groups [41] coming from the starting $Bi(NO_3)_3$ used to**

synthetize BiOCl powders. The bands at 1615 and 3550 cm^{-1} are the deformation vibration and stretching vibration of the hydroxyl group (-OH) [44]. Most of these signals, as well as -OH, were not detected after annealing.

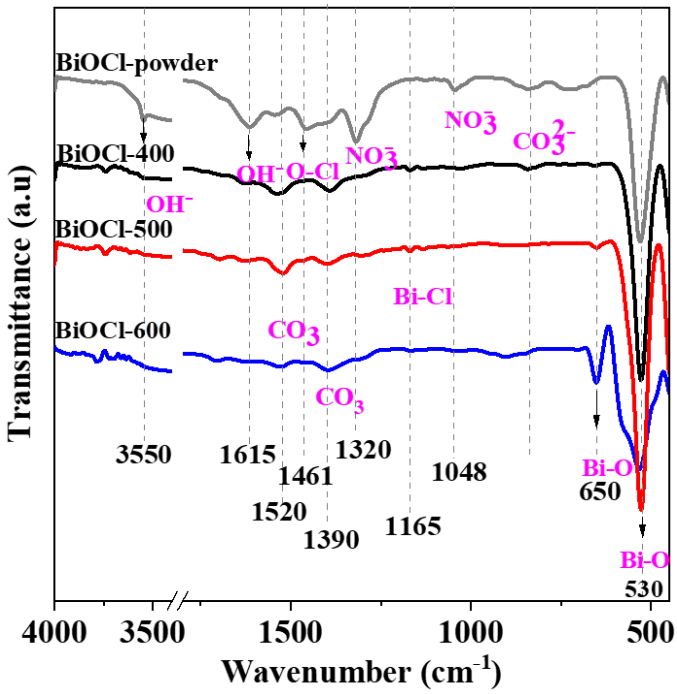

Fig. 7. FTIR spectra for the BiOCl films obtained at different sintering temperatures.

3.3. Dye adsorption studies

To investigate the capability of the BiOCl films to adsorb dye molecules for potential application as a photoanode in DSSC, the absorbance spectra of dye sensitized BiOCl films were measured.

Figure 8 shows the absorbance spectra of Rhodamine B and sensitized BiOCl films for immersion times of 8, 12 and 24 h. The constant lines correspond to the BiOCl films before dye sensitization. Fig. 8 a) shows the absorbance spectra of pure Rhodamine B (100 ppm in

ethanol), where the characteristic absorption peak at 551 nm is observed [45]. Figure 8 b) shows the absorbance spectra for the BiOCl-400 sample after sensitization, where it is possible to observe an absorption peak located at 574 nm. An increase in the absorbance from 0.37 to 0.42 can also be seen, as the immersion time increases from 8 h to 24 h. For the BiOCl-500 sample (see Fig 8 c)), the absorption peak is located at 569 nm, **and a maximum absorbance** of 0.47 is observed after 24 h of immersion.

Figure 8 d) shows the absorbance spectra for the BiOCl-600 sample, where an absorption peak located at 566 nm is observed, with a maximum absorbance of 0.24 after 24 h of immersion. **The BiOCl-600 sample showed the lowest dye adsorption, which could be a consequence of both the drastic reduction of the specific surface area when the BiOCl was sintered at 600 °C and the transformation to $Bi_{24}O_{31}Cl_{10}$. This reduced specific surface area provides fewer available sites for dye anchoring, negatively affecting the capability of BiOCl to be sensitized with rhodamine B.**

All the absorption spectra of sensitized films showed a bathochromic shift (~ 20 nm) and an increase in the width of peaks, which can be ascribed to the protonation of the dye and formation of *J*-aggregates as a consequence of the dye adsorption on the BiOCl surface [46, 47]. Protonation improves the electrostatic attraction between the negatively charged dye molecules and the positively charged semiconductor surface, thus may enhance dye adsorption **[48].** *J*-aggregates are known because they exhibit relevant optical properties, both fast exciton energy migration and efficient exciton coupling, which are important for light harvesting on photovoltaic devices [49]. Accordingly, all the obtained BiOCl films are capable to be sensitized with Rhodamine B, where the BiOCl-400 sample exhibited the highest absorbance after sensitization.

Based on the above results it is evident that the conditions of the sintering process influence morphology, chemical composition, structural properties, optical characteristics and adsorption capability of dye on BiOCl film.

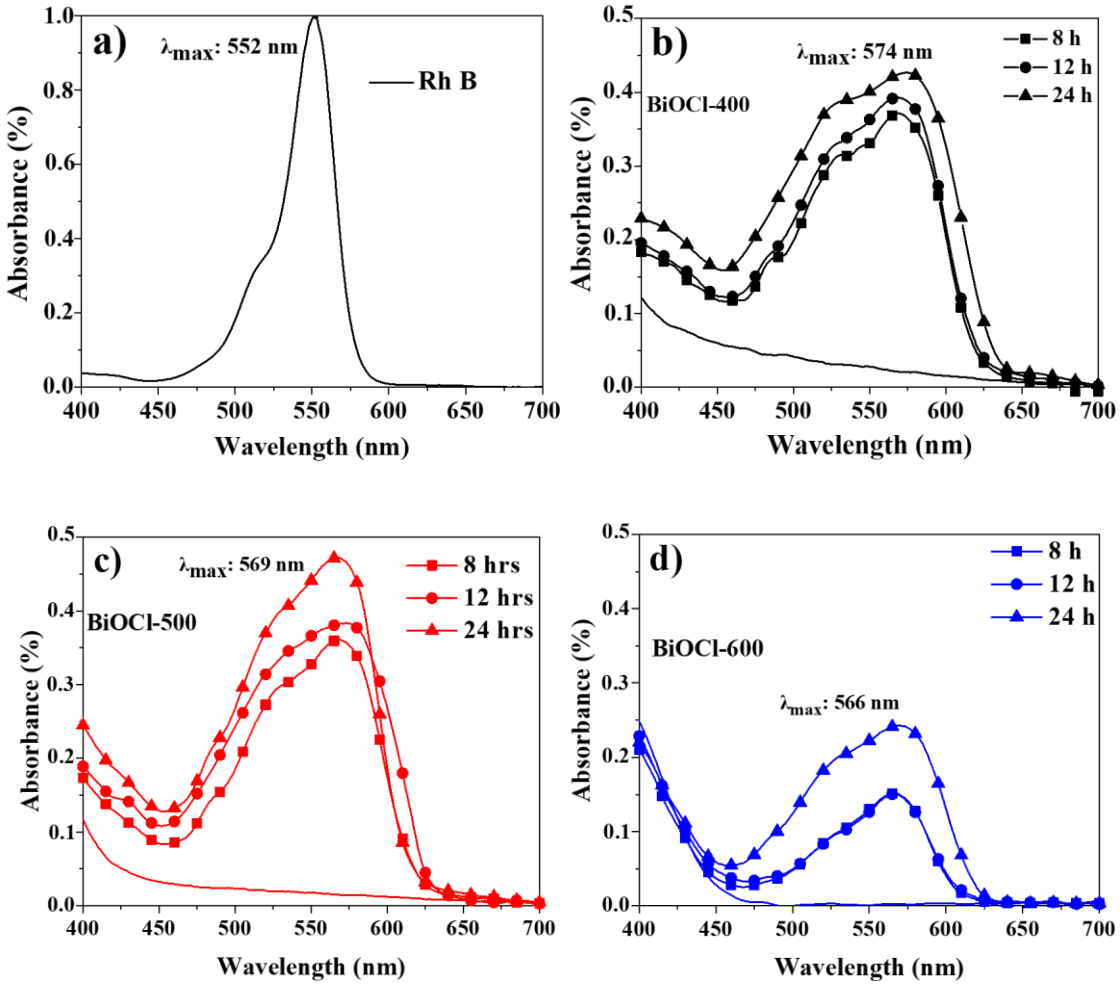

Fig. 8. Absorbance spectra for a) Rhodamine B in ethanol and dye sensitized BiOCl films sintered at b) 400 °C, c) 500 °C and d) 600 °C.

Conclusions

The effect of sintering temperature on the properties of BiOCl films obtained by the tape-casting method was studied. From the results, it is possible to conclude that a sintering temperature of 300ºC was not enough for eliminating the solvents used during

the production of the films. For sintering temperatures of 400, 500 and 600 ºC the following observations can be highlighted:

- **A morphological change from flakes-like particles (400 and 500 ºC) to rectangular ones (600ºC) was observed as the temperature increased. A surface area diminution of around 60% was observed as temperature increased.**
- **The chlorine content of the films diminished from 17 to 11 at. % when the sintering temperature changed from 400 to 600ºC.**
- **Phases transformations were observed as the sintering temperature increased. Small quantities of Bi_2O_3 were found in film sintered at 400ºC, which increased at 500ºC. At 600ºC the entire BiOCl film was transformed to $Bi_{24}O_{31}Cl_{10}$. Consequently, the band gap was reduced from 3.03 eV in films sintered at 400ºC to 2.8 eV in films sintered at 600ºC.**
- **The adsorption of Rhodamine B dye molecules decreased as the sintering temperature increased, which is due to both the surface area diminution and the differences in phases conforming the films. Hence, samples sintered at 400 ºC allowed the maximum dye molecules adsorption.**

Therefore, by setting the sintering temperature it is possible to obtain BiOCl films with porous morphology, wide band gap and high dye molecules adsorption, which provides a new alternative semiconductor material to be used as a photoanode in DSSCs.

Credit authorship contribution statement

L. Pizarro-Castillo: Methodology, Validation, Investigation, Formal analysis, Writing-original draft, Visualization. **Adriana C. Mera:** Formal analysis, Resources. **G. Cabello-**

Guzmán: Resources. **C. Bernal**: Resources. **M. Bizarro**: Resources, Visualization. **C. Carrasco:** Conceptualization, Writing-review & editing, Supervision. **María-Jesús Blesa**: Formal analysis, Visualization. **C.A. Rodríguez:** Conceptualization, Methodology, Investigation, Resources, Formal analysis, Writing-review & editing, Supervision, Project administration, Funding acquisition.

Acknowledgments

The authors acknowledge the National Agency for Research and Development by funding this research through the International Cooperation Program PCI-REDES Project N° 180038 and Solar Energy Research Center (SERC) FONDAP project No. 15110019. L. Pizarro acknowledges ANID for financing his Ph.D. studies (grant Doctorado Nacional 21220791). C.A. Rodríguez also acknowledges the financial support given by the University of La Serena through the DIDULS project N° PR19538513, project ID1953852 and project "FIULS 2030" N° 18ENI2-104235 from the "*Nueva Ingeniería para el 2030 en Regiones - Etapa de Implementación*" program funded by CORFO. María-Jesús Blesa acknowledges the financial support from the Spanish Ministry of Science and Innovation-MCIN/ AEI /10.13039/501100011033 (Project PID2019-104307GB-I00) and Gobierno de Aragón-Fondo Social Europeo (E47_20R).

References

[1] K. Kakiage, Y. Aoyama, T. Yano, K. Oya, J. I. Fujisawa, & M. Hanaya, Highly-efficient dye-sensitized solar cells with collaborative sensitization by silyl-anchor and carboxy-anchor dyes. Chem. Commun. 51 (2015), 15894–15897. https://doi.org/10.1039/c5cc06759f

[2] D. Kishore Kumar, J. Kříž, N. Bennett, B. Chen, H. Upadhayaya, K. R. Reddy & V. Sadhu, Functionalized metal oxide nanoparticles for efficient dye-sensitized solar cells (DSSCs): A review. Mater. Sci. Energy. Technol. 3 (2020), 472–481. https://doi.org/10.1016/j.mset.2020.03.003

[3] B. Kilic, Produce of carbon nanotube/ZnO nanowires hybrid photoelectrode for efficient dye-sensitized solar cells. J. Mater. Sci–Mater. Electron. 30 (2019), 3482-3487. https://doi.org/10.1007/s10854-018-00624-y

[4] J. Lee, N. Park, & Y. Shin, Solar Energy Materials & Solar Cells Nano-grain SnO_2 electrodes for high conversion efficiency SnO_2–DSSC, Sol. Energy. Mater. Sol. Cells. 95 (2011), 179–183. https://doi.org/10.1016/j.solmat.2010.04.027

[5] R. Abdul, A. Sabirin, J. Subbiah, J. Zhen, & K. Kalantar-zadeh, Highly ordered anodized Nb_2O_5 nanochannels for dye-sensitized solar cells. Electrochem. Commun. 40 (2014), 20–23. https://doi.org/10.1016/j.elecom.2013.12.011

[6] P. Jayabal, V. Sasirekha, J. Mayandi, K. Jeganathan, & V. Ramakrishnan, A facile hydrothermal synthesis of $SrTiO_3$ for dye sensitized solar cell application. J. Alloys. Comp. 586 (2014), 456–461. https://doi.org/10.1016/j.jallcom.2013.10.012

[7] J. Wu, X. Cao, Growth of bismuth oxyhalide nanoplates on self-standing TiO_2 nanowire film exhibiting enhanced photoelectrochemical performances. Electrochim. Acta. 247

(2017), 646-656. https://doi.org/10.1016/j.electacta.2017.07.026

[8] S. Wu, C. Wang, Y. Cui, T. Wang, B. Huang, X. Zhang, P. Brault, Synthesis and photocatalytic properties of BiOCl nanowire arrays. Mater. Lett. 64 (2010), 115–118. https://doi.org/10.1016/j.matlet.2009.10.010

[9] Y. Myung, F. Wu, S. Banerjee, J. Park, & P. Banerjee, Electrical conductivity of p-type BiOCl. Chem. Commun. 21 (2015), 2629-2632. https://doi.org/10.1039/C4CC09295C

[10] J. Song, Q. Fan, W. Zhu, R. Wang & Z. Dong, Preparation of BiOCl with high specific surface area and excellent visible light photocatalytic activity. Mat. Lett. 165 (2016), 14–18. https://doi.org/10.1016/j.matlet.2015.11.093

[11] X. Liu, Y. Su, Q. Zhao, C. Du & Z. Liu, Constructing $Bi_{24}O_{31}Cl_{10}$/BiOCl heterojunction via a simple thermal annealing route for achieving enhanced photocatalytic activity and selectivity. Sci. Rep. 6 (2016), 28689. https://doi.org/10.1038/srep28689

[12] H. Li, S. Xu, Z. Huang, J. Huang, J. Wang, L. Zhang, C. Zhang, Facet-dependent nonlinear optical properties of bismuth oxychloride single-crystal nanosheets, J. Mater. Chem. C. 6 (2018), 8709–8716. https://doi.org/10.1039/c8tc01613e

[13] P. Cui, J. Wang, Z. Wang, J. Chen, X. Xing, L. Wang & R. Yu, Bismuth oxychloride hollow microspheres with high visible light photocatalytic activity. Nano Res. 9 (2016), 593–601. https://doi.org/10.1007/s12274-015-0939-z

[14] K. Xu, Z. Xu, L. Wang, H. Feng, F. Pan, J. Zhuang, Y. Du & W. Hao, First-principles study on the electronic structures and diffusion behaviors of intrinsic defects in BiOCl. Comput. Mater. Sci. 203 (2022), 111088. https://doi.org/10.1016/j.commatsci.2021.111088

[15] **C. Cao, L. Xiao, C. Chen & Q. Cao. Synthesis of novel Cu_2O/BiOCl heterojunction nanocomposites and their enhanced photocatalytic activity under visible light. Appl Surf Sci. 357 (2015), 1171-1179. https://doi.org/10.1016/j.apsusc.2015.09.121**

[16] **M. Shakeel Ahmad, A. K. Pandey & N. Abd Rahim. Advancements in the development of TiO_2 photoanodes and its fabrication methods for dye sensitized solar cell (DSSC) applications. A review. Renewable Sustainable Energy Rev. 77 (2017), 89-108. http://dx.doi.org/10.1016/j.rser.2017.03.129**

[17] **L. Yosefi & M. Hoghighi. Sequential precipitation design of p-BiOCl-p-Mn_3O_4 binary semiconductor nanoheterojunction with enhanced photoactivity for acid orange 7 removal from water. Ceram Int. 45 (2019), 8248-8257. https://doi.org/10.1016/j.ceramint.2019.01.130**

[18] **A. khalifa, S. Shafie, W. Z. W. Hasan, H. N. Lim, M. Rusop, S. S. Pandey, A. K. Vats, H. A. AlSultan & B. Samaila, Comprehensive performance analysis of dye-sensitized solar cells using single layer TiO_2 photoanode deposited using screen printing technique. *Optik*. 223 (2020), 165595. https://doi.org/10.1016/j.ijleo.2020.165595**

[19] **A. Agrawal, S. A. Siddiqui, A. Soni, K. Khandelwal & G. D. Sharma, Performance analysis of TiO_2 based dye sensitized solar cell prepared by screen printing and doctor blade deposition techniques. Sol. Energy. 226 (2021), 9–19. https://doi.org/10.1016/j.solener.2021.08.001**

[20] A. A. Putri, S. Kato, N. Kishi & T. Soga, Study of annealing temperature effect on the photovoltaic performance of BiOI-based materials. Appl. Sci. 9 (2019), 3342. https://doi.org/10.3390/app9163342

[21] A. Luz, J. Conradt, M. Wolff, H. Kalt & C. Feldmann, P-DSSCs with BiOCl and BiOBr semiconductor and polybromide electrolyte. Solid State Sci. 19 (2013), 172–177. https://doi.org/10.1016/j.solidstatesciences.2013.02.021

[22] L. Wang, J. Shang, W. Hao, S. Jiang, S. Huang, T. Wang, Z. Sun, Y. Du, S. Dou, T. Xie, D. Wang & J. Wang, A dye-sensitized visible light photocatalyst-$Bi_{24}O_{31}Cl_{10}$. Sci. Rep. 4 (2014), 7384. https://doi.org/10.1038/srep07384

[23] J. M. Montoya-Zamora, A. Martínez-de la Cruz & E. L. Cuéllar, Synthesis of BiOI photocatalyst by microwave method using EDTA as retarder of the reaction. Res. Chem. Intermed. 43 (2017), 2545–2563. https://doi.org/10.1007/s11164-016-2779-1

[24] S. Landi, I. R. Segundo,E. Freitas, M. Vasilevskiy, J. Carneiro & C. J. Tavares, Use and misuse of the Kubelka-Munk function to obtain the band gap energy from diffuse reflectance measurements. Solid State Commun. 341 (2022), 1–7. https://doi.org/10.1016/j.ssc.2021.114573

[25] A. B. Marco, N. Martínez de Baroja, J. M. Andrés-Castán, S. Franco, R. Andreu, B. Villacampa, J. Orduna & J. Garín, Pyranylidene/thienothiophene-based organic sensitizers for dye-sensitized solar cells. Dyes Pigm. 161 (2019), 205–213. https://doi.org/10.1016/j.dyepig.2018.09.035

[26] F. Deng, X. Lu, F. Zhong, X. Pei, X. Luo, S. Luo, C. Au, Fabrication of 2D sheet-like BiOCl / carbon quantum dot hybrids via a template-free coprecipitation method and their tunable visible-light photocatalytic activities derived from different size distributions of carbon quantum dots. Nanotechnology, 27 (2016), 0657701. https://doi.org/10.1088/0957-4484/27/6/065701

[27] J. Ma, J. Ding, L. Yu, L. Li, Y. Kong, S. Komarneni, BiOCl dispersed on NiFe – LDH leads to enhanced photo-degradation of Rhodamine B dye. Appl. Clay Sci. 109-110 (2015), 76–82. https://doi.org/10.1016/j.clay.2015.02.009

[28] S. Cao, C. Guo, Y. Lv & Y. Guo, A novel BiOCl film with flowerlike hierarchical structures and its optical. Nanotechnology. 20 (2009), 275702. https://doi.org/10.1088/0957-4484/20/27/275702

[29] H. Li, S. Xu, Z. Huang, J. Huang, J. Wang, L. Zhang, C. Zhang, Facet-dependent nonlinear optical properties of bismuth oxychloride single-crystal nanosheets, J. Mater. Chem. C. 6 (2018), 8709–8716. https://doi.org/10.1039/c8tc01613e

[30] C. A. Rodríguez, M. G. Sandoval-Paz, R. Saavedra, C. Trejo-Cruz, F. De La Carrera, L. E. Aragon, M. Sirena, M.P. Delplancke & C. Carrasco, Comprehensive study of growth mechanism and properties of low Zn content $Cd_{1-x}Zn_xS$ thin films by chemical bath. Mater. Res. 19 (2016), 1335–1343. https://doi.org/10.1590/1980-5373-MR-2015-0660

[31] J. I. Langford & A. J. C. Wilson, Scherrer after sixty years: A survey and some new results in the determination of crystallite size. J. Appl. Crystalligr. 11 (1978),102-113. https://doi.org/10.1107/S0021889878012844

[32] **N. Abdul Karim, U. Mehmood, H. Fizza Zahid & T. Asif. Nanostructured photoanode and counter electrode materials for efficient Dye-Sensitized Solar Cells (DSSCs). Sol Energy. 185 (2019), 165-188. https://doi.org/10.1016/j.solener.2019.04.057**

[33] C. A. Rodríguez, A. Delgadillo, J. Núñez, G. Cabello-Guzmán, A. C. Mera, M. P. Delplancke, B. Villacampa & C. Carrasco, Effect of supporting electrolyte concentration on one-step electrodeposited CuInS2 films for ZnS/$CuInS_2$ solar cell applications. J. Solid State

Electrochem. 24 (2020), 1405–1414. https://doi.org/10.1007/s10008-020-04622-1

[34] P. Cui, J. Wang, Z. Wang, J. Chen, X. Xing, L. Wang & R. Yu, Bismuth oxychloride hollow microspheres with high visible light photocatalytic activity. Nano Res. 9 (2016), 593–601. https://doi.org/10.1007/s12274-015-0939-z

[35] C. Gomez, O. De Pablos-Rivera, J. Medina, P. Silva-Bermudez, S. Muhl, A. Zeinert, S. Rodil, Stabilization of the delta-phase in Bi_2O_3 thin films, Solid States Ionics, 255 (2014), 147–152. https://doi.org/10.1016/j.ssi.2013.12.027

[36] L. A. Klinkova, V. I. Nikolaichik, N. V. Barkovskii & V. K. Fedotov, Thermal stability of $Bi2O_3$. Russ. J. of Inorg. Chem. 52 (2017), 1822–1829. https://doi.org/10.1134/S0036023607120030

[37] P. Cui, J. Wang, Z. Wang, J. Chen, X. Xing, L. Wang & R. Yu, Bismuth oxychloride hollow microspheres with high visible light photocatalytic activity. Nano Res. 9 (2016), 593–601. https://doi.org/10.1007/s12274-015-0939-z

[38] J. Hou, D. Dai, R. Wei, X. Wu, X. Wang, M. Tahir & J. J. Zou, Narrowing the Band Gap of BiOCl for the Hydroxyl Radical Generation of Photocatalysis under Visible Light. ACS Sustainable Chem. Eng. 7 (2019), 16569–16576. https://doi.org/10.1021/acssuschemeng.9b03885

[39] L. Zhao, X. Zhang, C. Fan, Z. Liang & P. Han, First-principles study on the structural, electronic and optical properties of BiOX (X=Cl, Br, I) crystals. Phys. B: Condens Matt. 407 (2012), 3364–3370. https://doi.org/10.1016/j.physb.2012.04.039

[40] K. Masula, Y. Bhongiri, G. Raghav Rao, P. Vijay Kumar, S. Pola, & M. Basude, Evolution of photocatalytic activity of CeO_2–Bi_2O_3 composite material for wastewater

degradation under visible-light irradiation. Opt. Mater. 106 (2022), 112201. https://doi.org/10.1016/j.optmat.2022.112201

[41] R. P. Oertel, R. A. Plane, Raman and Infrared study on nitrate complexes of Bismuth (III). Inorg. Chem. 7 (1968), 1192-1196.

[42] E.A. Abdullah, A.H. Abdullah, Z. Zainal, M. Z. Hussein, T.K. Ban. Bismuth Basic Nitrate as a novel adsorbent for azo dye removal. E-J. Chem. 9 (2012), 1885-1896. https://doi.org/10.1155/2012/617050

[43] Z. S. Seddigi, M. A. Gondal, U. Baig, S. A. Ahmed, M. A. Abdulaziz, E. Y. Danish, Facile synthesis of light harvesting semiconductor bismuth oxychloride nano photo-catalysts for efficient removal of hazardous organic pollutants. Plos One. 12 (2017), https://doi.org/10.1371/journal.pone.0172218

[44] T. Xie, L. Xu, C. Liu, J. Yang & M. Wang, Magnetic composite BiOCl-$SrFe_{12}O_{19}$: A novel p-n type heterojunction with enhanced photocatalytic activity. Dalton Trans. 43 (2014), 2211–2220. https://doi.org/10.1039/c3dt52219a

[45] P. K. Baviskar, J. B. Zhang, V. Gupta, S. Chand & B.R. Sankapal, Nanobeads of zinc oxide with rhodamine B dye as a sensitizer for dye sensitized solar cell application. J. Alloys Comp. 510 (2011), 33–37. https://doi.org/10.1016/j.jallcom.2011.08.034

[46] T. Kitamura, M. Ikeda, K. Shigaki, T. Inoue, N. A. Anderson, X. Ai, T. Lian & S. Yanagida, Phenyl-Conjugated Oligoene Sensitizers for TiO_2 Solar Cells. Chem Mater. 16 (2004), 1806–1812. https://doi.org/10.1021/cm0349708

[47] H. Tian, X. Yang, R. Chen, R. Zhang, A. Hagfeldt & L. Sun, Effect of different dye baths and dye-structures on the performance of dye-sensitized solar cells based on

triphenylamine dyes. J. Phys. Chem. C, 112 (2008), 11023–11033. https://doi.org/10.1021/jp800953s

[47] Z. Sheng Wang, & G, Zhou. Effect of surface protonation of TiO_2 on charge recombination and conduction band edge movement in dye-sensitized solar eells. J. Phys. Chem. C. 113 (2009), 15417–15421. https://doi.org/10.1021/jp905366t

[48] **M. S. A. Abdel-Mottaleb, M. M. S. Abdel-Mottaleb, H. S. Hafez, M. Saif, J-Aggregates of Amphiphilicic Cyanine Dyes-Sensitized solar cells: A combination betweem computational chemistry and experimental device physics. Int. J. Photoenergy. (2014), 579476. https://doi.org/10.1155/2014/579476**

The effect of sintering temperature on the properties of the BiOCl films for potential application in DSSC

L. Pizarro-Castillo[1], Adriana C. Mera[2,3], G. Cabello-Guzmán[4], C. Bernal[2,5], M. Bizarro[6], C. Carrasco[1], María-Jesús Blesa[7], C. A. Rodríguez[2,3*]

1 Thin film and electrochemical processes laboratory, Department of Materials Engineering, Faculty of Engineering, Universidad de Concepción. 270 Edmundo Larenas St., Concepción 4070409, Chile.

2 Multidisciplinary Research Institute for Science and Technology, Universidad de La Serena, 1305 Raúl Bitrán Av., La Serena, 1700000, Chile.

3 Department of Chemistry, Faculty of Science, Universidad de La Serena, 1305 Raúl Bitrán Av., La Serena, 1700000, Chile.

4 *Department of Basic Sciences, Faculty of Sciences, Universidad del Bío-Bío, Campus Fernando May, 720 Andres Bello St., 3784444, Chillán, Chile.*

5 Departamento de Ingeniería de Alimentos, Facultad de Ingeniería, Universidad de La Serena, 1305 Raúl Bitrán Av., La Serena, 1700000, Chile.

6 Instituto de Investigaciones en Materiales, Universidad Nacional Autónoma de México, Circuito Exterior S/N, Ciudad Universitaria, Coyoacán, 04510, Ciudad de México, México.

7 Departamento de Química Orgánica, INMA, Universidad de Zaragoza-CSIC, 50009, Zaragoza, Spain.

* *Corresponding author. E-mail address: arodriguez@userena.cl*

TEL:+56-9-84775538

Abstract

In this work, BiOCl films were obtained by tape casting using BiOCl powders synthesized by the co-precipitation method. The effect of the film's sintering temperature (300°C to 600°C) on the morphology, chemical composition, crystalline phases and optical characteristics was studied. The obtained BiOCl powders showed a flake-like morphology, a tetragonal crystalline structure without secondary phases and a wide band gap of 3.53 eV. For BiOCl films, results indicated that as the sintering temperature increased the flake-like shaped particles changed to rectangular ones while the amount of chlorine in the films decreased. A phase transition from tetragonal BiOCl to monoclinic $Bi_{24}O_{31}Cl_{10}$ was also observed as the sintering temperature increased. Consequently, optical studies revealed that the band gap of BiOCl films decreased from 3.03 eV to 2.82 eV. FTIR analysis demonstrated that the organic groups were removed from the films only for sintering temperatures above 400 °C. The Rhodamine B dye adsorption capacity of BiOCl films decreased with increasing sintering temperature. The results obtained allow us to conclude that BiOCl films are suitable for use in DSSC when the sintering temperature is in the range of 400 to 500 ºC.

Keywords: BiOCl films, tape casting, Dye-sensitized solar cells.

1. Introduction

Dye-sensitized solar cells (DSSC) have emerged as a simple and low-cost alternative to traditional silicon-based solar cells. So far, the highest Power Conversion Efficiency (PCE) for commonly TiO_2-based DSSC is close to 14.3 % [1]. Increasing this value is one of the main challenges of DSSC devices for future industrial production. Hence, new semiconductor materials capable of increasing the adsorption of dye molecules, reducing recombination processes and improving charge-carrier transport are needed [2]. Several semiconductors have been studied as a potential replacement for TiO_2, such as ZnO [3], SnO_2 [4], Nb_2O_5 [5] and $SrTiO_3$ [6]; however, none of them has significantly improved the efficiency of TiO_2-based DSSC.

Bismuth oxychloride (BiOCl) is a relatively new semiconductor material that has received much attention due to its similarity to TiO_2 [7]. BiOCl is an indirect semiconductor with a wide band gap (3.2 - 3.5 eV [8]) and a light absorption edge close to 360 nm that would ensure light transmission to the dye molecules if used in DSSC [9, 10]. The internal structure of BiOCl consists of $[Bi_2O_2]^{2+}$ layers intercalated by two slabs of Cl atoms, which provides this material a favorable transfer and separation of photogenerated charge carriers [11]. This unique layered structure gives the material excellent physical and chemical properties, allowing its application in different fields such as solar cells, photocatalysts and photoelectrochemical studies [12, 13]. Furthermore, theoretical studies have shown that BiOCl exhibits suitable band edge positions to collect electrons from different organic compounds [14].

Not only the optical and structural properties of the semiconductor are important for obtaining an efficient DSSC, but also the morphological characteristics play an important

role to evaluate the dye molecules adsorption [15]. It is known that semiconductor films used in DSSC must have a porous morphology for large adsorption of dye molecules on their surface [16]. Although several physical and chemical methods are available to obtain semiconductor films, most of them lead to compact morphology instead of a porous one [17]. Commonly, the synthesis of porous semiconductor films for DSSC application is carried out employing the Screen Printing method [18, 19] or Tape Casting [20]. In these two methods, an annealing process is required to tune the particle size and phase composition, which ultimately determines the textural material properties. Therefore, the study of the effect of the annealing process on the film properties is crucial to controlling both the composition and the morphology of the film for DSSC application.

As far as we know, only few works have reported the synthesis and use of BiOCl films as a semiconductor material in DSSCs [21, 22]. Some attempts have been done for this purpose. Luz et al. obtained BiOCl and BiOBr nanodiscs (100-150 nm in diameter, 15-25 nm in thickness) by water-based nucleation. In order to control particle growth and shape particles, the nanodiscs were purified by a complex phase-transfer reaction. The prepared BiOCl film was used in a p-DSSC device sensitized with coumarin and a PCE of 0.003% was achieved [21]. In 2014, Wang et al. reported a DSSC based on the $Bi_{24}O_{31}Cl_{10}$ semiconductor sensitized with the N719 dye. Nevertheless, this material exhibited a relatively low band gap of 2.2 eV, which lead to an absorption of visible light, limiting the light absorption by dye molecules [22]. Hence, the challenge of obtaining BiOCl films with suitable characteristics to be used in DSSCs remains.

The aim of this paper is to study the effect of sintering temperature on the BiOCl properties to be used as a semiconductor in DSSC. BiOCl powder was synthesized by a simple co-

precipitation method and films were obtained by the tape-casting method. These films were heat-treated at temperatures of 300°C, 400°C, 500°C and 600 °C. Morphology, microstructure and optical characteristics of BiOCl films are measured and related to the adsorption of dye molecules, specifically, Rhodamine B.

2. Experimental Details

2.1 Synthesis of BiOCl powder

BiOCl powder was synthetized by the co-precipitation method according to the procedure represented in Figure 1 a) to c). 0.29 g of KCl (99.0 %, Merck®) was dissolved in 40 mL of deionized water and stirred for 30 min. A second solution containing 1.97 g of $Bi(NO_3)_3 \times 5H_2O$ (99.0 %, Sigma-Aldrich®) was dissolved in 40 mL of 10 % acetic acid solution and stirred for 30 min (see Fig. 1 a). Subsequently, the KCl solution (4 mM) was added dropwise to the bismuth solution (4 mM) under stirring (Fig. 1 b). After the total incorporation of both solutions, the reaction mixture was kept under constant stirring for 30 min at room temperature. The resulting product was collected by gravity filtration and washed with ethanol and deionized water successively. The resulting powder was dried at 60 °C for 12 h (Fig. 1c) [23].

2.2 Synthesis of BiOCl films

BiOCl films were deposited on glass substrates using the tape-casting technique. First, the substrates were cleaned with water and soap and subsequently rinsed with deionized water and ethanol. Cleaned substrates were dried in an oven at 60 °C for 30 min. Then, to deposit the BiOCl film, an exposed area of 0.5 × 0.5 cm was delimited by using Kapton tape®.

Secondly, the BiOCl paste was prepared by mixing 0.5 g of BiOCl powder, 0.4 g of polyvinylpyrrolidone (PVP, 10.000 mol wt, Sigma-Aldrich®) and 0.7 mL of ethanol (99.5%, Emplura®) as graphically shown in Fig. 1 d). After 15 min of continuous mixing, 0.3 mL of α-terpineol (96%, Sigma-Aldrich®) was added and mixed for 5 min (Fig. 1 e). Afterward, as shown in Fig. 1 f), the paste was deposited on the glass substrate by spreading it on the substrate surface with a squeegee.

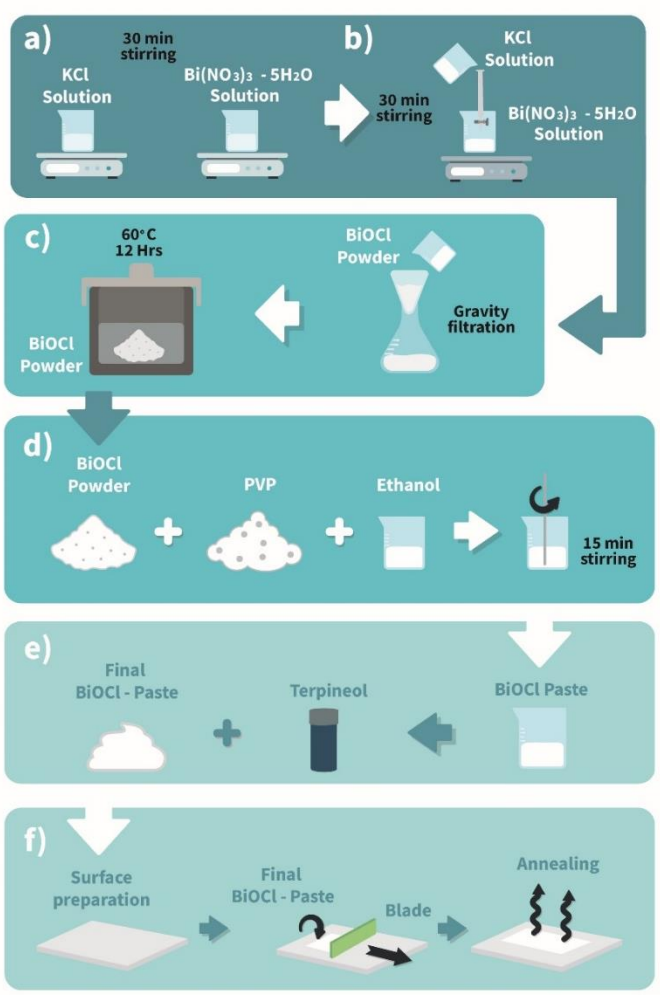

Fig. 1. Synthesis of a) to c) BiOCl powder by co-precipitation method; d) to f) BiOCl films by tape casting.

The obtained samples were kept at room temperature for 5 min, and after, the Kapton tape was removed. The obtained samples were sintered in air in a tubular furnace (MPTI corporation GSL–1100X).

Four different sintering conditions were tested, which are shown in Table 1. These temperatures of sintering were selected to eliminate organic additives and solvents used during the BiOCl films synthesis [19]. The sintered samples were removed from the furnace when the temperature was lower than 50 °C and stored in dry and dark conditions.

Table 1. Sintering conditions for BiOCl films

Experiment Nº	**Sample**	**Temperature (ºC)**	**Time (min)**
1	BiOCl 300	300	180
2	BiOCl 400	400	180
3	BiOCl 500	500	30
4	BiOCl 600	600	30

2.3 Characterization of BiOCl powders and films

Surface characteristics and semi-quantitative chemical composition of the BiOCl samples were evaluated using scanning electron microscopy (SEM) and energy dispersive spectroscopy (EDS), using a Hitachi Su 70 microscope with an EDS detector attached to the equipment. The specific surface area and the pore size distribution of the samples were obtained by N_2 adsorption–desorption analysis, using a Micromeritics ASAP 2020 instrument and applying Brunauer-Enmmets-Teller (BET) and Barret-Joyner-Halenda (BJH)

methods. The crystalline phases of BiOCl powders and films were identified by X-ray diffraction (XRD) using a Rigaku Ultim IV diffractometer with Cu Kα radiation (λ = 1.5406 A). The samples were measured at the scanning rate of 0.5°/min in the 2θ scan range of 5° - 65° at 40 kV and 40 mA. Optical characteristics of the obtained samples were studied through diffuse reflectance spectroscopy (DRS) in the wavelength interval of 340–800 nm using a UV-Vis spectrophotometer Thermo Scientific model Evolution 220; the optical band gap was calculated through the Kubelka-Munk method [24]. Finally, Fourier transform infrared (FTIR) spectra were obtained using a PerkinElmer spectrometer model Spectrum Two with $LiTaO_3$ MIR detector.

2.4 Dye adsorption studies on BiOCl films

The dye adsorption capability of the BiOCl films was investigated with the method previously reported by Marco *et al*. by the absorbance spectra of sensitized transparent BiOCl films [25]. Glass substrates with an exposed area of 2.5 × 2.5 cm^2 were cleaned as described in section 2.2. Subsequently, 250 μL of BiOCl paste (0.5 g of BiOCl powder, 0.4 g of PVP, 1.5 mL of ethanol and 0.3 mL of α-terpineol) was spread on the glass substrate by tape casting. The obtained transparent films were sintered at the conditions detailed in Table 1.

For dye adsorption, the obtained transparent BiOCl films were immersed in a Rhodamine B solution (1.37×10^{-3} M) for 8, 12 and 24 h. After the corresponding time, samples were removed from the solution, washed with ethanol, and dried at room temperature. Dye-sensitized BiOCl samples were kept in dark conditions to avoid dye degradation. Absorption spectra of sensitized BiOCl films were measured in the wavelength interval of 340–800 nm using a UV-VIS spectrophotometer ThermoScientific Evolution 220.

3. Results and Discussion

3.1. Characterization of BiOCl powder

Figure 2 a) shows the SEM images for the BiOCl powder obtained by the co-precipitation method, where flake-like shape particles are observed. It can also be seen that the flakes are forming agglomerates with a size of ~ 1μm. Deng *et al*. and Ma *et al*. reported similar morphology for BiOCl powder obtained by the co-precipitation method [26, 27]. The semi-quantitative chemical composition of the BiOCl powder, measured by EDS, showed the presence of Bi (38.1%), O (24.1%) and Cl (37.8%) with a Bi:O:Cl ratio of 1:0.7:1 that could mean that samples have oxygen vacancies.

Figure 2 b) shows the XRD diffractograms, where the polycrystalline nature of the obtained BiOCl powder can be seen. Peak identification reveals the tetragonal phase of BiOCl according to the Powder Diffraction File (PDF) from the International Centre for Diffraction Data (ICDD) N° 06-0249 [28,29]. A peak widening is observed, which can be attributed to small crystallite size and/or inhomogeneous deformations in the powders. To determine the reason for the widening of the peaks, Williamson-Hall (W-H) relation was applied, which is given by Eq. (1) [30]:

$$\beta \cos\theta = \frac{K\lambda}{D} + 4\varepsilon sin\theta \qquad (1)$$

where D is the average crystallite size, λ is the X-ray wavelength (0.154056 nm), k is the shape factor (0.75 in this case [31]), β is the full width at half maximum (FWHM) of the diffraction peaks, ε is the lattice microstrain and θ is the diffraction angle.

Figure 2 c) shows the Williamson-Hall plot, which is obtained by plotting $4sin(\theta)$ along the x-axis and $\beta cos(\theta)$ along the y-axis. From the linear fit to the data, the crystallite size was

estimated from the *y*-intercept and the lattice strain from the slope. The obtained value for D was 22 nm which indicates the nanocrystalline nature of the synthesized BiOCl powders. The microstrain was found to be 1.75×10^{-3}, indicating that the lattice strain practically does not contribute to peak broadening [28]. The presence of these lattice deformations could be a consequence of the oxygen atom vacancies revealed by EDS analysis.

The optical band gap of the BiOCl powder was calculated using the Tauc plot through the Kubeka-Munk model for diffuse reflectance [24]. Figure 2 d) shows the Tauc plot, where a band gap value of 3.53 ± 0.03 eV is extracted, which agrees with the value reported previously for BiOCl powders [29]. An optical band gap higher than 3.0 eV ensures that most of the incident light is not being absorbed by the semiconductor, which is an optimal condition to be considered as a potential photoanode in DSSC [32].

3.2. Characterization of BiOCl films

Figure 3 shows photographs of the BiOCl films before and after the heat treatments. The obtained sample prior annealing process is shown in Fig. 3 a), where it is possible to observe a homogeneous and white film, which is characteristic of BiOCl material. In Fig. 3 b) it is shown that after sintering at 300 °C, a dark BiOCl film was obtained. This indicates that the organic additives and solvents used during the film deposition were not completely evaporated and/or burning during the heat treatment. The presence of these organic compounds reduces the exposition of the semiconductor surface to the dye molecules and blocks the light transmission towards the dye. For this reason, this sample was discarded and not subjected to further characterization.

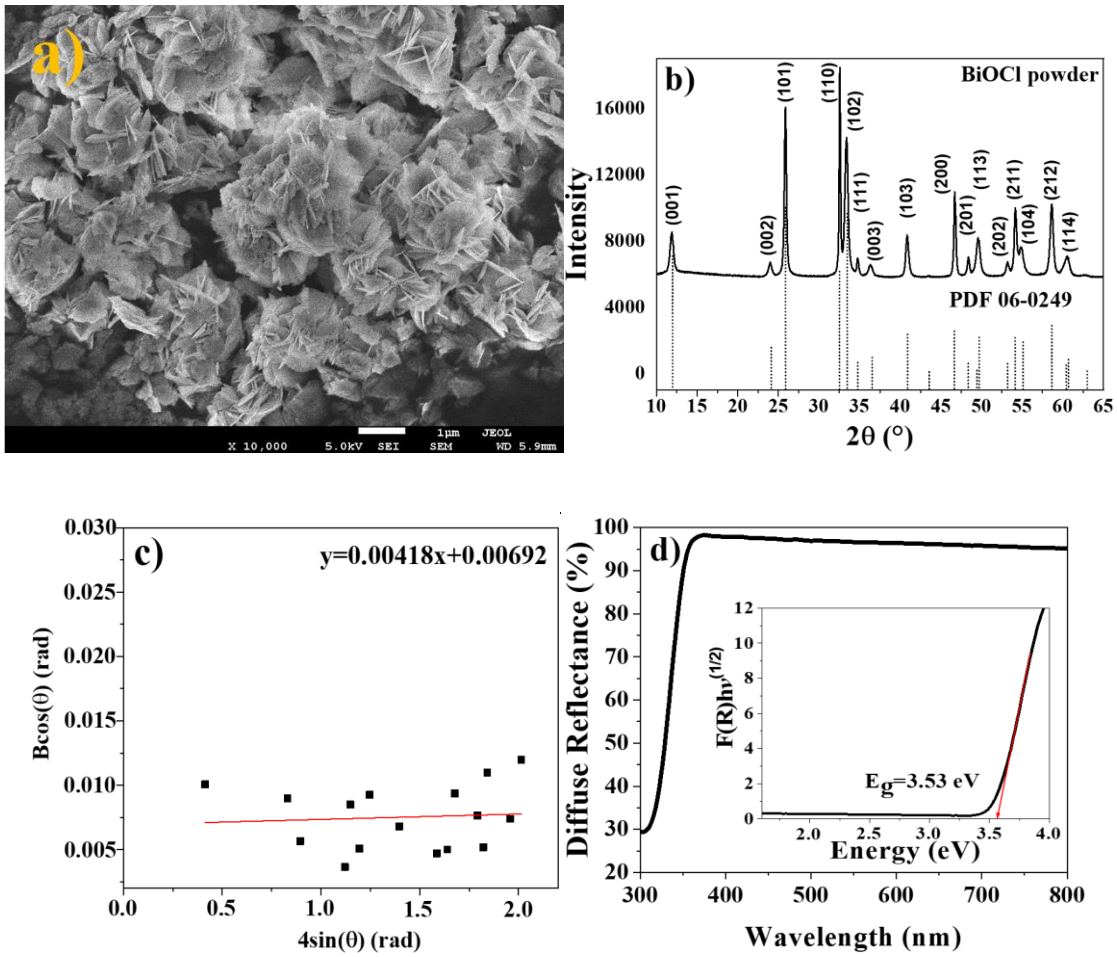

Fig. 2. BiOCl powder obtained by co-precipitation method: a) SEM image, b) XRD pattern, c) W-H plot, d) Tauc plot.

Fig. 3 c) depicts the BiOCl sample sintered at 400 °C where is seen that the obtained film exhibits a white color meaning that all the organic additives and solvents were removed after 3 h of calcination. For samples sintered at 500 °C and 600 °C, Fig. 3 d and e, respectively, the films exhibited a white color after 30 min of annealing. From Fig. 3 c) to e), it can be seen the tendency of the films to become slightly yellowish as the sintering temperature increases, which could be related to possible structural and/or chemical modifications.

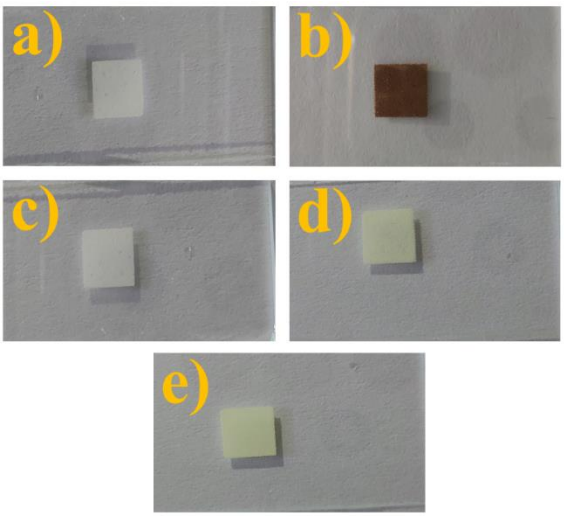

Fig. 3. BiOCl films: a) without heat treatment, heat treated at b) 300ºC (BiOCl 300), c) 400ºC (BiOCl 400), d) 500ºC (BiOCl 500) and d) 600ºC (BiOCl 600).

The surface morphology of the BiOCl films sintered at different temperatures is shown in Fig. 4. Figure 4 a) and b) show the surface characteristics of the BiOCl-400 sample. A highly porous morphology with flake-like shaped particles that are linked to each other forming spherical aggregates is observed. It can be noticed that the particle shape for the BiOCl-400 sample is similar to the one observed for the BiOCl powders. It is highlighted that the highly porous morphology observed would favor the dye molecules adsorption on the semiconductor surface.

The surface morphology of the BiOCl-500 sample is shown in Fig. 4 c) and d), where a more compact film than the BiOCl-400 sample is observed. In addition, some cracks are seen on the sample surface (see yellow arrow), which could be attributed to a possible phase transformation in the films involving crystalline structure changes and deformations [33, 34]. Figure 4 e) and f) shows the morphology of the BiOCl-600 sample, where it is observed that the sintering at a temperature of 600 °C leads to the appearance of broad cracks on the sample

surface. In addition, the flake-like shaped particles observed in the BiOCl-400 and BiOCl-500 samples changed to rectangular with rounded edges, resulting in a more compact surface. This morphological modification could be associated with the changes in the chemical composition of the films, which are shown in Table 2. The increase in temperature leads to a shrinkage of the films because of the reduction of chlorine in the samples, which corresponds with previous reports [20].

From Table 2, it is also observed that in all samples an increase in the sintering temperature produces a diminution in chlorine concentration.

To reach a further understanding of the effect of sintering temperature on the surface characteristics, the specific surface area of the BiOCl powders thermally treated at 400, 500 and 600º C was measured. It must be noted that the specific surface area on films is not possible to be measured, and the values for BiOCl powders are presented only for comparison purposes. The results showed that the specific surface area for BiOCl powder sintered at 400 °C, 500 °C and 600 °C were 17.05 ± 0.11, 19.55 ± 0.09 and 6.02 ± 0.07 m^2/g, respectively, and the pore volume was 0.054, 0.054 and 0.017 cm^3/g, respectively. Hence, the BiOCl annealed at 600 °C exhibited the lowest surface area, which is consistent with the morphological change observed in Fig. 4.

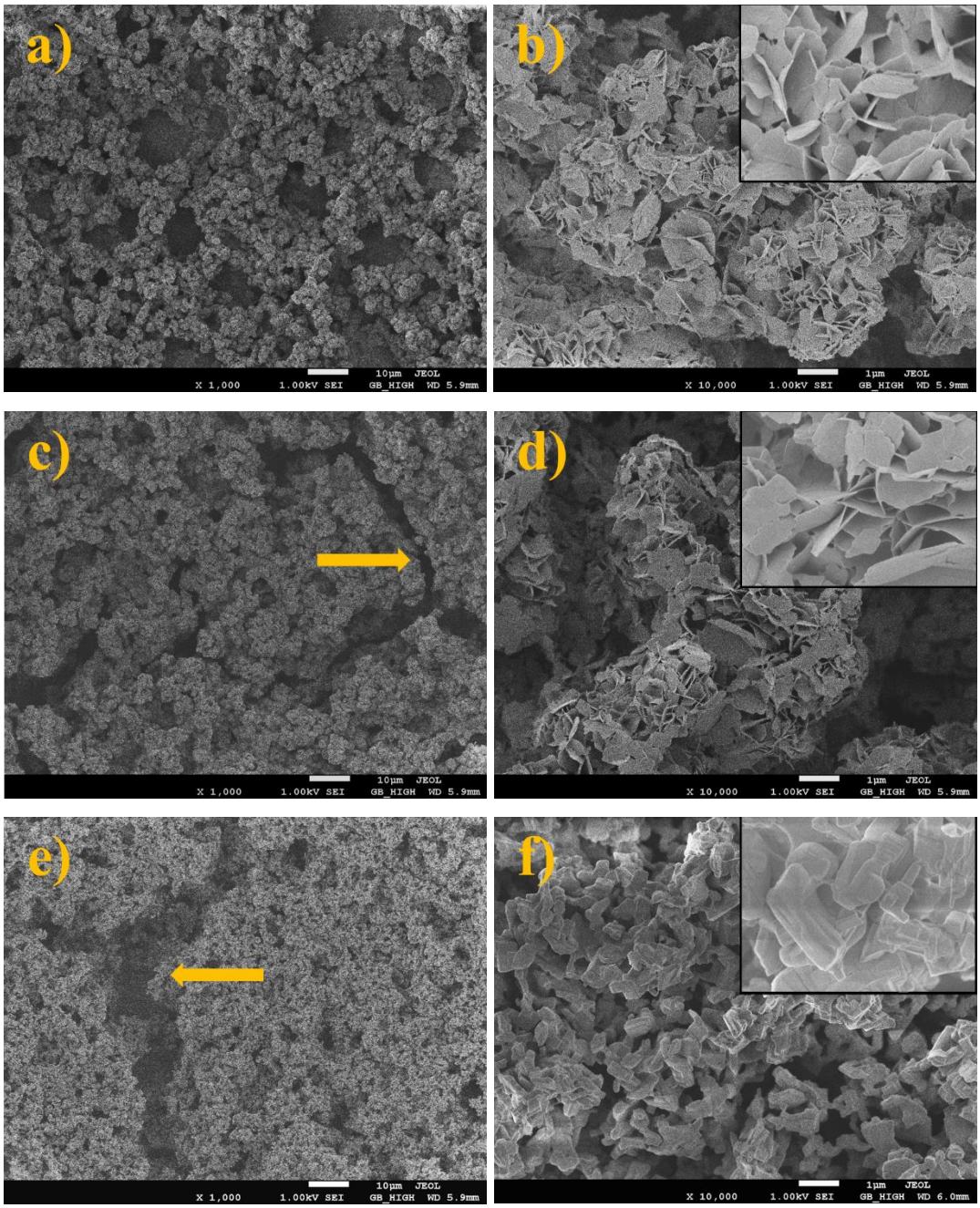

Fig. 4. SEM images of sintered BiOCl films at different temperatures: (a-b) 400 °C, (c-d) 500 °C and (e-f) 600 °C.

Table 2. Semi-quantitative EDS chemical composition of obtained sintered films.

Sample	**Bi (% at.)**	**O (% at.)**	**Cl (% at.)**	**Bi: O: Cl**
BiOCl 400 °C	35.7 ± 1.3	46.7 ± 1.9	17.6 ± 0.7	1: 1.30: 0.49
BiOCl 500 °C	38.7 ± 1.3	45.3 ± 1.9	16.0 ± 0.7	1: 1.17: 0.41
BiOCl 600 °C	40.3 ± 1.3	48.4 ± 1.9	11.3 ± 0.7	1: 1.20: 0.30

Figure 5 shows the XRD pattern of BiOCl films after sintering at (a) 400, (b) 500 and (c) 600 °C. From the diffractogram of the BiOCl-400 sample (Fig. 4 a), the presence of several diffraction peaks is observed, which can be ascribed to both the tetragonal phase of BiOCl (star symbol) according to the PDF N° 06-0249 and the tetragonal phase of Bi_2O_3 (circle symbol) according to the PDF N° 29-0236. The appearance of Bi_2O_3 is a consequence of the chlorine volatilization during the sintering process, and therefore the crystal phase becomes unstable undergoing a phase transformation from pure BiOCl to a mixture of Bi_2O_3 and BiOCl. [35].

When the sintering temperature is increased up to 500 °C (see Fig. 5 b), the appearance of several diffraction peaks is observed, which can be ascribed to the tetragonal phase of Bi_2O_3 according to the PDF N° 29-0236. When comparing the XRD pattern for BiOCl-400 with BiOCl-500 samples, a partial phase transformation from BiOCl to Bi_2O_3 is observed. This change could be attributed to the chlorine reduction during the sintering. It has been reported that, among their four polymorphs, the tetragonal phase of Bi_2O_3 is the predominant one after annealing at temperatures up to 643 °C [36], which agrees with the finding in these samples.

In Fig. 5 c) the XRD pattern for the BiOCl-600 sample is shown. It is possible to observe a drastic change in the diffraction pattern when the sintering temperature was 600 °C. The diffraction peaks can be attributed to the monoclinic phase of $Bi_{24}O_{31}Cl_{10}$ according to the PDF N° 75-0887. The phase transformation observed as the sintering temperature increases as a consequence of the continuous chlorine volatilization. Thus, the heat treatment allowed the continued reduction of chlorine to Cl_2, leading to a phase transformation in two stages: (a) the appearance of the Bi_2O_3 phase at 400°C and 500 °C, and (b) change from the tetragonal lattice of BiOCl to the monoclinic lattice of $Bi_{24}O_{31}Cl_{10}$ at 600 °C [11, 37]. These findings are in accordance with the atomic chemical composition shown in Table 2, where the atomic composition of the BiOCl-400 sample can be adjusted to a mixture of BiOCl (52.8 %) and Bi_2O_3 (47.2 %); similarly, the BiOCl-500 sample corresponds to a mixture of BiOCl (48 %) and Bi_2O_3 (52 %). On the contrary, the atomic composition of the BiOCl-600 sample corresponds only to the single phase of $Bi_{24}O_{31}Cl_{10}$.

The crystallite size of BiOCl films was calculated by using Scherrer's equation, due to films obtained at 400 ° and 500 °C were a mixture of Bi_2O_3 and BiOCl phases, thus the near position of peaks involve overlaps the points on the Williamson-Hall graph. The crystallite size values were 19, 13 and 30 nm for BiOCl samples annealed at 400 °C, 500 °C and 600 °C, respectively. This behavior could be attributed to the phase change from BiOCl to $Bi_{24}O_{31}Cl_{10}$ as the sintering temperature increased from 400 °C to 600 °C. The sample annealed at 500 °C exhibits a broadening peak with a reduction of the crystallite size as a consequence of the increase in lattice disorder, while at 600 °C an increase in the crystallite size was observed.

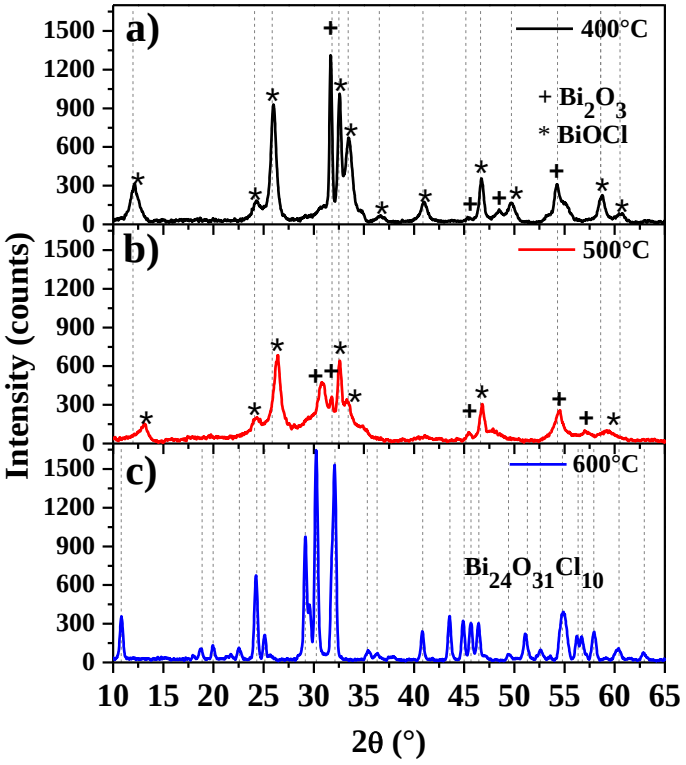

Fig 5. Diffraction patterns of films heat treated at (a) 400 °C, (b) 500 °C and (c) 600 °C.

Figure 6 shows the Tauc plot obtained from the diffuse reflectance spectra through the Kubelka-Munk method. By extrapolating the linear portion of the Tauc plot, the band gap values for BiOCl films are obtained, where it is seen that the band gap values tend to decrease as the sintering temperature increases. The reduction in the band gap can be attributed to the phase transformation with rising temperature. Thus, the BiOCl-400 sample has a band gap value of 3.03 ± 0.01 eV which agrees with the expected value for BiOCl [38, 39]. For the BiOCl-500 sample, the band gap value exhibits a reduction up to 2.87± 0.06 eV, which is very close to the band gap value for Bi_2O_3 (E_g=2.87) [40]. The BiOCl-600 sample exhibits a band gap value of 2.80± 0.01 eV, which agrees with the value for the $Bi_{24}O_{31}Cl_{10}$ phase (Eg=2.7-2.8 eV) [11, 36].

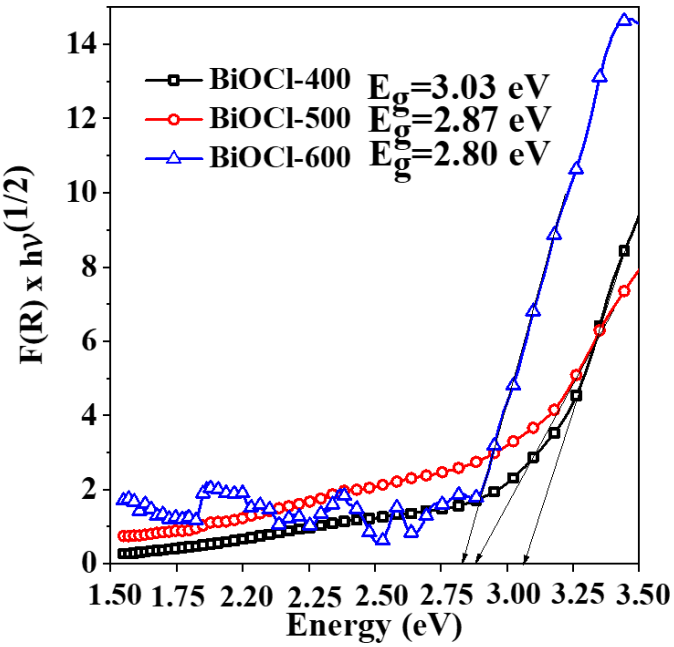

Fig. 6. Tauc plot of BiOCl films.

The FTIR spectra of BiOCl powder, BiOCl-400, BiOCl-500 and BiOCl-600 samples are presented in Fig. 7. All the samples showed the band at 530 cm^{-1}, which corresponds to the symmetrical stretching vibration of Bi-O bond [41-42]. The band at 650 cm^{-1} is also assigned to the Bi-O bond [41, 43], which increases with the annealing temperature and is seen in the sample annealed at 600 °C. The small band located at 1461 cm^{-1} in the powder sample is attributed to O-Cl vibration and the band slightly perceptible at 1165 cm^{-1} corresponds to the Bi-Cl bond. The signals at 530 and 650 cm^{-1} for the BiOCl-600 sample are observed to be more intense than BiOCl-400 and BiOCl-500 samples, which can be attributed to the phases present in the samples.

Moreover, it can be observed that the BiOCl powder sample contains some remaining organic groups from the precursors used during the co-precipitation method. The bands at 1050 and 1320 cm^{-1} are ascribed to NO_3^- groups [41] coming from the starting $Bi(NO_3)_3$ used to

synthetize BiOCl powders. The bands at 1615 and 3550 cm^{-1} are the deformation vibration and stretching vibration of the hydroxyl group (-OH) [44]. Most of these signals, as well as -OH, were not detected after annealing.

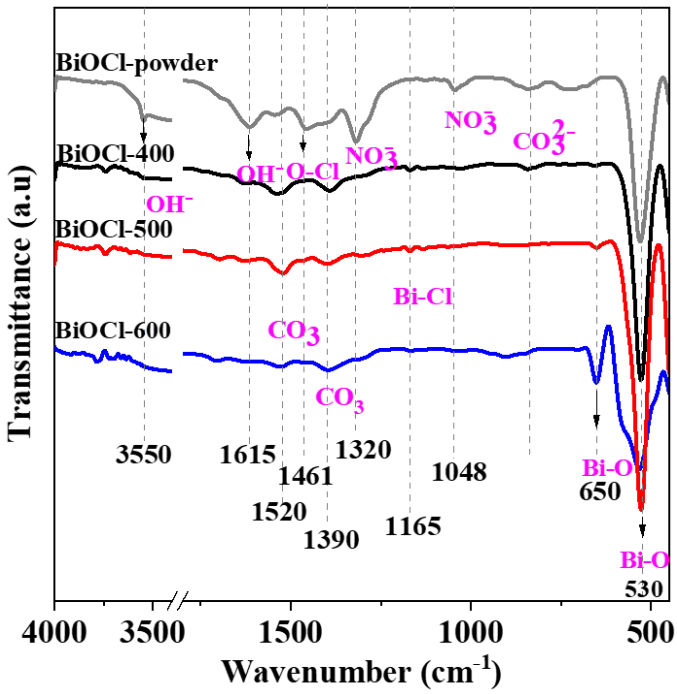

Fig. 7. FTIR spectra for the BiOCl films obtained at different sintering temperatures.

3.3. Dye adsorption studies

To investigate the capability of the BiOCl films to adsorb dye molecules for potential application as a photoanode in DSSC, the absorbance spectra of dye sensitized BiOCl films were measured.

Figure 8 shows the absorbance spectra of Rhodamine B and sensitized BiOCl films for immersion times of 8, 12 and 24 h. The constant lines correspond to the BiOCl films before dye sensitization. Fig. 8 a) shows the absorbance spectra of pure Rhodamine B (100 ppm in

ethanol), where the characteristic absorption peak at 551 nm is observed [45]. Figure 8 b) shows the absorbance spectra for the BiOCl-400 sample after sensitization, where it is possible to observe an absorption peak located at 574 nm. An increase in the absorbance from 0.37 to 0.42 can also be seen, as the immersion time increases from 8 h to 24 h. For the BiOCl-500 sample (see Fig 8 c)), the absorption peak is located at 569 nm, and a maximum absorbance of 0.47 is observed after 24 h of immersion.

Figure 8 d) shows the absorbance spectra for the BiOCl-600 sample, where an absorption peak located at 566 nm is observed, with a maximum absorbance of 0.24 after 24 h of immersion. The BiOCl-600 sample showed the lowest dye adsorption, which could be a consequence of both the drastic reduction of the specific surface area when the BiOCl was sintered at 600 °C and the transformation to $Bi_{24}O_{31}Cl_{10}$. This reduced specific surface area provides fewer available sites for dye anchoring, negatively affecting the capability of BiOCl to be sensitized with rhodamine B.

All the absorption spectra of sensitized films showed a bathochromic shift (~ 20 nm) and an increase in the width of peaks, which can be ascribed to the protonation of the dye and formation of *J*-aggregates as a consequence of the dye adsorption on the BiOCl surface [46, 47]. Protonation improves the electrostatic attraction between the negatively charged dye molecules and the positively charged semiconductor surface, thus may enhance dye adsorption [48]. *J*-aggregates are known because they exhibit relevant optical properties, both fast exciton energy migration and efficient exciton coupling, which are important for light harvesting on photovoltaic devices [49]. Accordingly, all the obtained BiOCl films are capable to be sensitized with Rhodamine B, where the BiOCl-400 sample exhibited the highest absorbance after sensitization.

Based on the above results it is evident that the conditions of the sintering process influence morphology, chemical composition, structural properties, optical characteristics and adsorption capability of dye on BiOCl film.

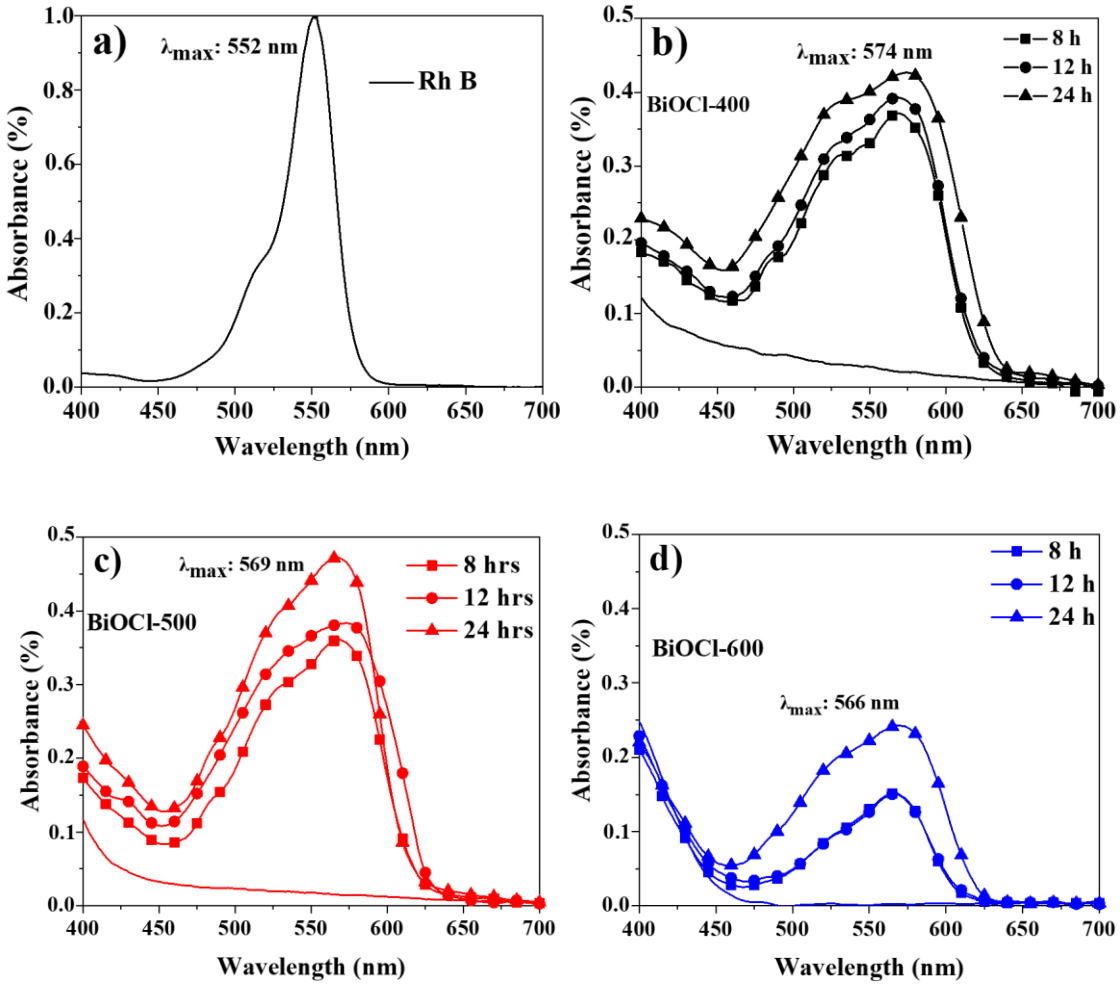

Fig. 8. Absorbance spectra for a) Rhodamine B in ethanol and dye sensitized BiOCl films sintered at b) 400 °C, c) 500 °C and d) 600 °C.

Conclusions

The effect of sintering temperature on the properties of BiOCl films obtained by the tape-casting method was studied. From the results, it is possible to conclude that a sintering temperature of 300ºC was not enough for eliminating the solvents used during the production

of the films. For sintering temperatures of 400, 500 and 600 ºC the following observations can be highlighted:

- A morphological change from flakes-like particles (400 and 500 ºC) to rectangular ones (600ºC) was observed as the temperature increased. A surface area diminution of around 60% was observed as temperature increased.
- The chlorine content of the films diminished from 17 to 11 at. % when the sintering temperature changed from 400 to 600ºC.
- Phases transformations were observed as the sintering temperature increased. Small quantities of Bi_2O_3 were found in film sintered at 400ºC, which increased at 500ºC. At 600ºC the entire BiOCl film was transformed to $Bi_{24}O_{31}Cl_{10}$. Consequently, the band gap was reduced from 3.03 eV in films sintered at 400ºC to 2.8 eV in films sintered at 600ºC.
- The adsorption of Rhodamine B dye molecules decreased as the sintering temperature increased, which is due to both the surface area diminution and the differences in phases conforming the films. Hence, samples sintered at 400 ºC allowed the maximum dye molecules adsorption.

Therefore, by setting the sintering temperature it is possible to obtain BiOCl films with porous morphology, wide band gap and high dye molecules adsorption, which provides a new alternative semiconductor material to be used as a photoanode in DSSCs.

Credit authorship contribution statement

L. Pizarro-Castillo: Methodology, Validation, Investigation, Formal analysis, Writing-original draft, Visualization. **Adriana C. Mera:** Formal analysis, Resources. **G. Cabello-**

Guzmán: Resources. **C. Bernal**: Resources. **M. Bizarro**: Resources, Visualization. **C. Carrasco:** Conceptualization, Writing-review & editing, Supervision. **María-Jesús Blesa**: Formal analysis, Visualization. **C.A. Rodríguez:** Conceptualization, Methodology, Investigation, Resources, Formal analysis, Writing-review & editing, Supervision, Project administration, Funding acquisition.

Acknowledgments

The authors acknowledge the National Agency for Research and Development by funding this research through the International Cooperation Program PCI-REDES Project N° 180038 and Solar Energy Research Center (SERC) FONDAP project No. 15110019. L. Pizarro acknowledges ANID for financing his Ph.D. studies (grant Doctorado Nacional 21220791). C.A. Rodríguez also acknowledges the financial support given by the University of La Serena through the DIDULS project N° PR19538513, project ID1953852 and project "FIULS 2030" N° 18ENI2-104235 from the "*Nueva Ingeniería para el 2030 en Regiones - Etapa de Implementación*" program funded by CORFO. María-Jesús Blesa acknowledges the financial support from the Spanish Ministry of Science and Innovation-MCIN/ AEI /10.13039/501100011033 (Project PID2019-104307GB-I00) and Gobierno de Aragón-Fondo Social Europeo (E47_20R).

References

[1] K. Kakiage, Y. Aoyama, T. Yano, K. Oya, J. I. Fujisawa, & M. Hanaya, Highly-efficient dye-sensitized solar cells with collaborative sensitization by silyl-anchor and carboxy-anchor dyes. Chem. Commun. 51 (2015), 15894–15897. https://doi.org/10.1039/c5cc06759f

[2] D. Kishore Kumar, J. Kříž, N. Bennett, B. Chen, H. Upadhayaya, K. R. Reddy & V. Sadhu, Functionalized metal oxide nanoparticles for efficient dye-sensitized solar cells (DSSCs): A review. Mater. Sci. Energy. Technol. 3 (2020), 472–481. https://doi.org/10.1016/j.mset.2020.03.003

[3] B. Kilic, Produce of carbon nanotube/ZnO nanowires hybrid photoelectrode for efficient dye-sensitized solar cells. J. Mater. Sci–Mater. Electron. 30 (2019), 3482-3487. https://doi.org/10.1007/s10854-018-00624-y

[4] J. Lee, N. Park, & Y. Shin, Solar Energy Materials & Solar Cells Nano-grain SnO_2 electrodes for high conversion efficiency SnO_2–DSSC, Sol. Energy. Mater. Sol. Cells. 95 (2011), 179–183. https://doi.org/10.1016/j.solmat.2010.04.027

[5] R. Abdul, A. Sabirin, J. Subbiah, J. Zhen, & K. Kalantar-zadeh, Highly ordered anodized Nb_2O_5 nanochannels for dye-sensitized solar cells. Electrochem. Commun. 40 (2014), 20–23. https://doi.org/10.1016/j.elecom.2013.12.011

[6] P. Jayabal, V. Sasirekha, J. Mayandi, K. Jeganathan, & V. Ramakrishnan, A facile hydrothermal synthesis of $SrTiO_3$ for dye sensitized solar cell application. J. Alloys. Comp. 586 (2014), 456–461. https://doi.org/10.1016/j.jallcom.2013.10.012

[7] J. Wu, X. Cao, Growth of bismuth oxyhalide nanoplates on self-standing TiO_2 nanowire film exhibiting enhanced photoelectrochemical performances. Electrochim. Acta. 247

(2017), 646-656. https://doi.org/10.1016/j.electacta.2017.07.026

[8] S. Wu, C. Wang, Y. Cui, T. Wang, B. Huang, X. Zhang, P. Brault, Synthesis and photocatalytic properties of BiOCl nanowire arrays. Mater. Lett. 64 (2010), 115–118. https://doi.org/10.1016/j.matlet.2009.10.010

[9] Y. Myung, F. Wu, S. Banerjee, J. Park, & P. Banerjee, Electrical conductivity of p-type BiOCl. Chem. Commun. 21 (2015), 2629-2632. https://doi.org/10.1039/C4CC09295C

[10] J. Song, Q. Fan, W. Zhu, R. Wang & Z. Dong, Preparation of BiOCl with high specific surface area and excellent visible light photocatalytic activity. Mat. Lett. 165 (2016), 14–18. https://doi.org/10.1016/j.matlet.2015.11.093

[11] X. Liu, Y. Su, Q. Zhao, C. Du & Z. Liu, Constructing $Bi_{24}O_{31}Cl_{10}$/BiOCl heterojunction via a simple thermal annealing route for achieving enhanced photocatalytic activity and selectivity. Sci. Rep. 6 (2016), 28689. https://doi.org/10.1038/srep28689

[12] H. Li, S. Xu, Z. Huang, J. Huang, J. Wang, L. Zhang, C. Zhang, Facet-dependent nonlinear optical properties of bismuth oxychloride single-crystal nanosheets, J. Mater. Chem. C. 6 (2018), 8709–8716. https://doi.org/10.1039/c8tc01613e

[13] P. Cui, J. Wang, Z. Wang, J. Chen, X. Xing, L. Wang & R. Yu, Bismuth oxychloride hollow microspheres with high visible light photocatalytic activity. Nano Res. 9 (2016), 593–601. https://doi.org/10.1007/s12274-015-0939-z

[14] K. Xu, Z. Xu, L. Wang, H. Feng, F. Pan, J. Zhuang, Y. Du & W. Hao, First-principles study on the electronic structures and diffusion behaviors of intrinsic defects in BiOCl. Comput. Mater. Sci. 203 (2022), 111088. https://doi.org/10.1016/j.commatsci.2021.111088

[15] C. Cao, L. Xiao, C. Chen & Q. Cao. Synthesis of novel Cu_2O/BiOCl heterojunction nanocomposites and their enhanced photocatalytic activity under visible light. Appl Surf Sci. 357 (2015), 1171-1179. https://doi.org/10.1016/j.apsusc.2015.09.121

[16] M. Shakeel Ahmad, A. K. Pandey & N. Abd Rahim. Advancements in the development of TiO_2 photoanodes and its fabrication methods for dye sensitized solar cell (DSSC) applications. A review. Renewable Sustainable Energy Rev. 77 (2017), 89-108. http://dx.doi.org/10.1016/j.rser.2017.03.129

[17] L. Yosefi & M. Hoghighi. Sequential precipitation design of p-BiOCl-p-Mn_3O_4 binary semiconductor nanoheterojunction with enhanced photoactivity for acid orange 7 removal from water. Ceram Int. 45 (2019), 8248-8257. https://doi.org/10.1016/j.ceramint.2019.01.130

[18] A. khalifa, S. Shafie, W. Z. W. Hasan, H. N. Lim, M. Rusop, S. S. Pandey, A. K. Vats, H. A. AlSultan & B. Samaila, Comprehensive performance analysis of dye-sensitized solar cells using single layer TiO_2 photoanode deposited using screen printing technique. *Optik*. 223 (2020), 165595. https://doi.org/10.1016/j.ijleo.2020.165595

[19] A. Agrawal, S. A. Siddiqui, A. Soni, K. Khandelwal & G. D. Sharma, Performance analysis of TiO_2 based dye sensitized solar cell prepared by screen printing and doctor blade deposition techniques. Sol. Energy. 226 (2021), 9–19. https://doi.org/10.1016/j.solener.2021.08.001

[20] A. A. Putri, S. Kato, N. Kishi & T. Soga, Study of annealing temperature effect on the photovoltaic performance of BiOI-based materials. Appl. Sci. 9 (2019), 3342. https://doi.org/10.3390/app9163342

[21] A. Luz, J. Conradt, M. Wolff, H. Kalt & C. Feldmann, P-DSSCs with BiOCl and BiOBr semiconductor and polybromide electrolyte. Solid State Sci. 19 (2013), 172–177. https://doi.org/10.1016/j.solidstatesciences.2013.02.021

[22] L. Wang, J. Shang, W. Hao, S. Jiang, S. Huang, T. Wang, Z. Sun, Y. Du, S. Dou, T. Xie, D. Wang & J. Wang, A dye-sensitized visible light photocatalyst-$Bi_{24}O_{31}Cl_{10}$. Sci. Rep. 4 (2014), 7384. https://doi.org/10.1038/srep07384

[23] J. M. Montoya-Zamora, A. Martínez-de la Cruz & E. L. Cuéllar, Synthesis of BiOI photocatalyst by microwave method using EDTA as retarder of the reaction. Res. Chem. Intermed. 43 (2017), 2545–2563. https://doi.org/10.1007/s11164-016-2779-1

[24] S. Landi, I. R. Segundo,E. Freitas, M. Vasilevskiy, J. Carneiro & C. J. Tavares, Use and misuse of the Kubelka-Munk function to obtain the band gap energy from diffuse reflectance measurements. Solid State Commun. 341 (2022), 1–7. https://doi.org/10.1016/j.ssc.2021.114573

[25] A. B. Marco, N. Martínez de Baroja, J. M. Andrés-Castán, S. Franco, R. Andreu, B. Villacampa, J. Orduna & J. Garín, Pyranylidene/thienothiophene-based organic sensitizers for dye-sensitized solar cells. Dyes Pigm. 161 (2019), 205–213. https://doi.org/10.1016/j.dyepig.2018.09.035

[26] F. Deng, X. Lu, F. Zhong, X. Pei, X. Luo, S. Luo, C. Au, Fabrication of 2D sheet-like BiOCl / carbon quantum dot hybrids via a template-free coprecipitation method and their tunable visible-light photocatalytic activities derived from different size distributions of carbon quantum dots. Nanotechnology, 27 (2016), 0657701. https://doi.org/10.1088/0957-4484/27/6/065701

[27] J. Ma, J. Ding, L. Yu, L. Li, Y. Kong, S. Komarneni, BiOCl dispersed on NiFe – LDH leads to enhanced photo-degradation of Rhodamine B dye. Appl. Clay Sci. 109-110 (2015), 76–82. https://doi.org/10.1016/j.clay.2015.02.009

[28] S. Cao, C. Guo, Y. Lv & Y. Guo, A novel BiOCl film with flowerlike hierarchical structures and its optical. Nanotechnology. 20 (2009), 275702. https://doi.org/10.1088/0957-4484/20/27/275702

[29] H. Li, S. Xu, Z. Huang, J. Huang, J. Wang, L. Zhang, C. Zhang, Facet-dependent nonlinear optical properties of bismuth oxychloride single-crystal nanosheets, J. Mater. Chem. C. 6 (2018), 8709–8716. https://doi.org/10.1039/c8tc01613e

[30] C. A. Rodríguez, M. G. Sandoval-Paz, R. Saavedra, C. Trejo-Cruz, F. De La Carrera, L. E. Aragon, M. Sirena, M.P. Delplancke & C. Carrasco, Comprehensive study of growth mechanism and properties of low Zn content $Cd_{1-x}Zn_xS$ thin films by chemical bath. Mater. Res. 19 (2016), 1335–1343. https://doi.org/10.1590/1980-5373-MR-2015-0660

[31] J. I. Langford & A. J. C. Wilson, Scherrer after sixty years: A survey and some new results in the determination of crystallite size. J. Appl. Crystalligr. 11 (1978),102-113. https://doi.org/10.1107/S0021889878012844

[32] N. Abdul Karim, U. Mehmood, H. Fizza Zahid & T. Asif. Nanostructured photoanode and counter electrode materials for efficient Dye-Sensitized Solar Cells (DSSCs). Sol Energy. 185 (2019), 165-188. https://doi.org/10.1016/j.solener.2019.04.057

[33] C. A. Rodríguez, A. Delgadillo, J. Núñez, G. Cabello-Guzmán, A. C. Mera, M. P. Delplancke, B. Villacampa & C. Carrasco, Effect of supporting electrolyte concentration on one-step electrodeposited CuInS2 films for ZnS/$CuInS_2$ solar cell applications. J. Solid State

Electrochem. 24 (2020), 1405–1414. https://doi.org/10.1007/s10008-020-04622-1

[34] P. Cui, J. Wang, Z. Wang, J. Chen, X. Xing, L. Wang & R. Yu, Bismuth oxychloride hollow microspheres with high visible light photocatalytic activity. Nano Res. 9 (2016), 593–601. https://doi.org/10.1007/s12274-015-0939-z

[35] C. Gomez, O. De Pablos-Rivera, J. Medina, P. Silva-Bermudez, S. Muhl, A. Zeinert, S. Rodil, Stabilization of the delta-phase in Bi_2O_3 thin films, Solid States Ionics, 255 (2014), 147–152. https://doi.org/10.1016/j.ssi.2013.12.027

[36] L. A. Klinkova, V. I. Nikolaichik, N. V. Barkovskii & V. K. Fedotov, Thermal stability of $Bi2O_3$. Russ. J. of Inorg. Chem. 52 (2017), 1822–1829. https://doi.org/10.1134/S0036023607120030

[37] P. Cui, J. Wang, Z. Wang, J. Chen, X. Xing, L. Wang & R. Yu, Bismuth oxychloride hollow microspheres with high visible light photocatalytic activity. Nano Res. 9 (2016), 593–601. https://doi.org/10.1007/s12274-015-0939-z

[38] J. Hou, D. Dai, R. Wei, X. Wu, X. Wang, M. Tahir & J. J. Zou, Narrowing the Band Gap of BiOCl for the Hydroxyl Radical Generation of Photocatalysis under Visible Light. ACS Sustainable Chem. Eng. 7 (2019), 16569–16576. https://doi.org/10.1021/acssuschemeng.9b03885

[39] L. Zhao, X. Zhang, C. Fan, Z. Liang & P. Han, First-principles study on the structural, electronic and optical properties of BiOX (X=Cl, Br, I) crystals. Phys. B: Condens Matt. 407 (2012), 3364–3370. https://doi.org/10.1016/j.physb.2012.04.039

[40] K. Masula, Y. Bhongiri, G. Raghav Rao, P. Vijay Kumar, S. Pola, & M. Basude, Evolution of photocatalytic activity of CeO_2–Bi_2O_3 composite material for wastewater

degradation under visible-light irradiation. Opt. Mater. 106 (2022), 112201. https://doi.org/10.1016/j.optmat.2022.112201

[41] R. P. Oertel, R. A. Plane, Raman and Infrared study on nitrate complexes of Bismuth (III). Inorg. Chem. 7 (1968), 1192-1196.

[42] E.A. Abdullah, A.H. Abdullah, Z. Zainal, M. Z. Hussein, T.K. Ban. Bismuth Basic Nitrate as a novel adsorbent for azo dye removal. E-J. Chem. 9 (2012), 1885-1896. https://doi.org/10.1155/2012/617050

[43] Z. S. Seddigi, M. A. Gondal, U. Baig, S. A. Ahmed, M. A. Abdulaziz, E. Y. Danish, Facile synthesis of light harvesting semiconductor bismuth oxychloride nano photo-catalysts for efficient removal of hazardous organic pollutants. Plos One. 12 (2017), https://doi.org/10.1371/journal.pone.0172218

[44] T. Xie, L. Xu, C. Liu, J. Yang & M. Wang, Magnetic composite BiOCl-$SrFe_{12}O_{19}$: A novel p-n type heterojunction with enhanced photocatalytic activity. Dalton Trans. 43 (2014), 2211–2220. https://doi.org/10.1039/c3dt52219a

[45] P. K. Baviskar, J. B. Zhang, V. Gupta, S. Chand & B.R. Sankapal, Nanobeads of zinc oxide with rhodamine B dye as a sensitizer for dye sensitized solar cell application. J. Alloys Comp. 510 (2011), 33–37. https://doi.org/10.1016/j.jallcom.2011.08.034

[46] T. Kitamura, M. Ikeda, K. Shigaki, T. Inoue, N. A. Anderson, X. Ai, T. Lian & S. Yanagida, Phenyl-Conjugated Oligoene Sensitizers for TiO_2 Solar Cells. Chem Mater. 16 (2004), 1806–1812. https://doi.org/10.1021/cm0349708

[47] H. Tian, X. Yang, R. Chen, R. Zhang, A. Hagfeldt & L. Sun, Effect of different dye baths and dye-structures on the performance of dye-sensitized solar cells based on

triphenylamine dyes. J. Phys. Chem. C, 112 (2008), 11023–11033. https://doi.org/10.1021/jp800953s

[47] Z. Sheng Wang, & G, Zhou. Effect of surface protonation of TiO_2 on charge recombination and conduction band edge movement in dye-sensitized solar eells. J. Phys. Chem. C. 113 (2009), 15417–15421. https://doi.org/10.1021/jp905366t

[48] M. S. A. Abdel-Mottaleb, M. M. S. Abdel-Mottaleb, H. S. Hafez, M. Saif, J-Aggregates of Amphiphilicic Cyanine Dyes-Sensitized solar cells: A combination betweem computational chemistry and experimental device physics. Int. J. Photoenergy. (2014), 579476. https://doi.org/10.1155/2014/579476